Effect of Preparation Procedure and Composition of Catalysts based on Mn and Ce Oxides in the Simultaneous Removal of NO_X and o-DCB

J.A. Martín-Martín, J. Sánchez-Robles, M.P. González-Marcos, A. Aranzabal, J.R. González-Velasco

Group of Chemical Technologies for Environmental Sustainability

Dept. of Chemical Engineering, Faculty of Science and Technology

The University of the Basque Country, UPV/EHU; P.O. Box 644, E-48080 Bilbao, Spain

mp.gonzalezmarcos@ehu.es

Highlights

Better catalytic performance of co-precipitation than impregnation catalysts.

NO and o-DCB conversion above 80% are reached with high Mn content catalysts.

There is surface Mn-CeO_2 interaction in impregnation catalysts, but without formation of a solid solution.

Low Ce content improves physicochemical properties and catalytic performance.

CO_2 selectivity above 80% was obtained with all MnO_X-CeO_2 co-precipitation catalysts.

*Graphical Abstract

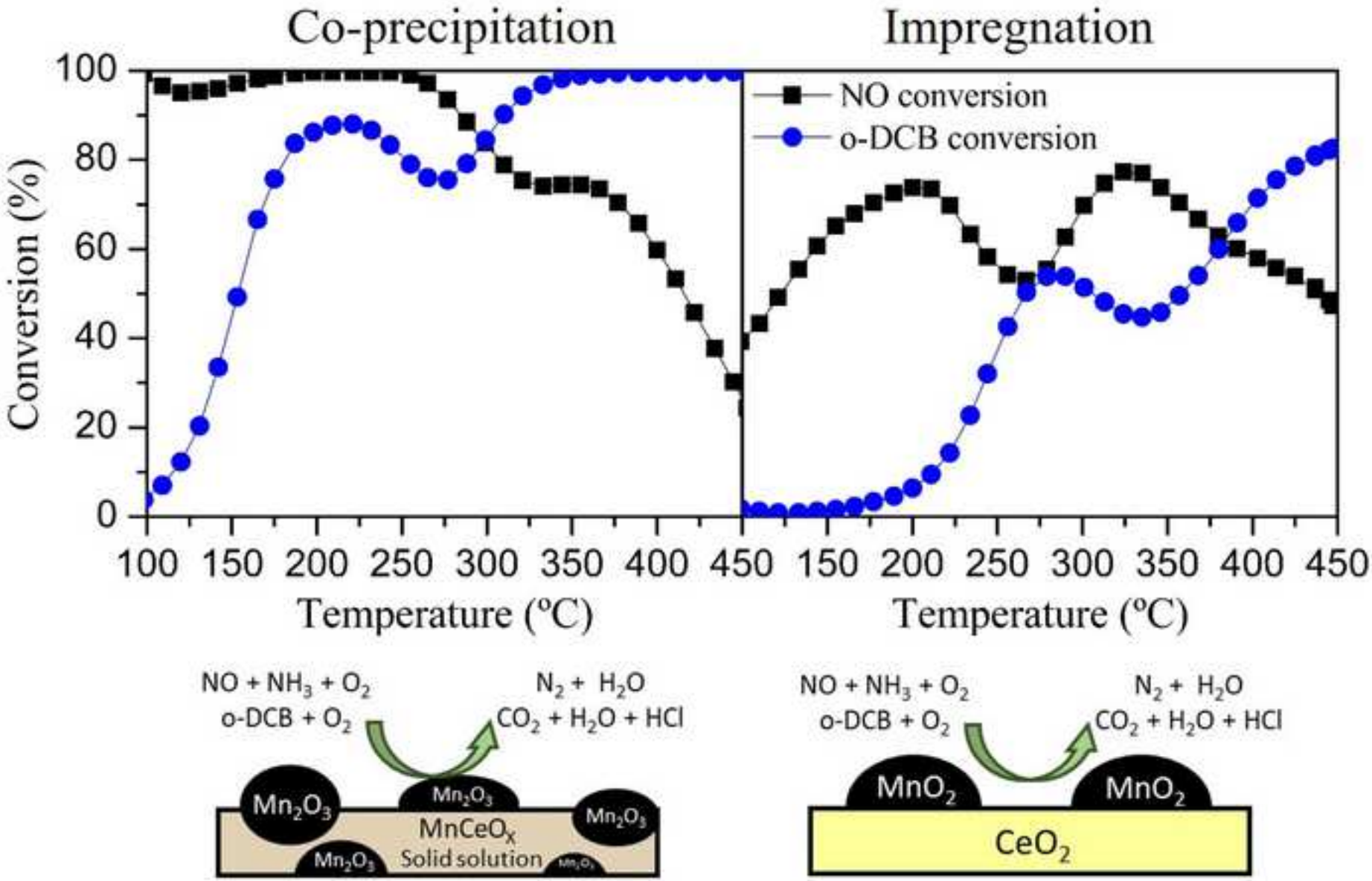

ABSTRACT

Two series of catalysts based on Mn and Ce oxides were prepared by co-precipitation and impregnation, in order to study their physicochemical properties and catalytic performance in the simultaneous reduction of NO and oxidation of o-DCB. Co-precipitation catalysts showed better activity than those prepared by impregnation because of the formation of a MnO_X-CeO_2 solid solution, which improves redox and acid properties. Moreover, the catalysts with MnO_X content between 80 and 90 mol.%, in which a coexistence between solid solution phase and Mn_2O_3 crystal was found, presented NO conversion above 90% at temperatures below 250 ºC and o-DCB conversion above 80% at temperatures above 200 ºC. The main by-products of SCR were N_2O, produced in the whole range of temperature, and NO_2, formed at temperatures above 300 ºC. Selectivity to CO_2 above 80% was obtained using co-precipitation catalysts in all temperature range. Deactivation experiments showed that oxidation reaction strongly contributes to deactivate impregnation catalysts, whereas the effect of deactivation is lower in co-precipitation catalysts at high Mn contents.

Keywords

MnO_X and CeO_2; Co-precipitation; Impregnation; o-DCB; NH_3-SCR.

1. INTRODUCTION

Simultaneous catalytic abatement of nitrogen oxides (NO_X) and polychlorinated dibenzo dioxins and furans (PCDD/Fs) is an alternative to the present techniques for elimination of both pollutants in municipal solid waste (MSW) incineration plants, in line with the continuous development of more efficient technologies due to the tightening of environment laws. In this process, both pollutants are removed in the same catalytic reactor [1,2]. The elimination of NO_X occurs through Selective Catalytic Reduction (SCR) with NH_3, while PCDD/Fs are removed by catalytic oxidation, according to:

$$4NO + 4NH_3 + O_2 \rightarrow 4N_2 + 6H_2O \quad (1)$$

$$C_{12}H_nCl_{8-n}O_2 + (9+0.5n)O_2 \rightarrow (n-4)H_2O + 12CO_2 + (8-n)HCl \quad (2)$$

This is a highly interesting process, since it combines the advantages of SCR, such as high efficiency and low cost, with those of catalytic oxidation, in which the pollutants are completely oxidized. This way, the use of other techniques, such as adsorption or absorption, which generate a waste that needs further treatment or disposal [2], is avoided.

Commercial catalysts for SCR are VO_X/TiO_2 promoted by WO_X or MoO_X [3,4]. The same catalysts are the main option for catalytic oxidation of PCDD/Fs and chlorinated benzenes [2], the latter commonly used as model compounds of PCDD/Fs for laboratory experiments, because they are safer to handle and have a similar structure. The fact that the same formulation is used for the removal of both types of pollutants is the key for this application in which NO_X and PCDD/Fs are removed simultaneously. Recently, Gallastegi-Villa et al. reported that the simultaneous abatement of NO and o-dichlorobenzene (o-DCB, model compound of PCDD/Fs) with VO_X/TiO_2 is possible [5]. However,

these catalysts are not efficient enough, because NO reduction occurs at lower temperatures than o-DCB oxidation, whereas NO conversion decreases at temperatures where o-DCB conversion is high [5].

Currently, SCR commercial systems are demanding to work at lower temperatures because they are located at the end of the cleaning gas line in order to avoid catalyst poisoning by SO_2 [6]. As a consequence, a reheat of the flue gas is needed up to the operating temperature of SCR reactor [7,8], which involves high costs. The development of alternative catalytic formulations is of great interest for decreasing operation temperature of SCR systems and obtaining oxidation of PCDD/Fs at lower temperatures.

In this sense, transition metals oxides (CuO_X, FeO_X, MnO_X, NiO_X, ZrO_X) as catalysts for low-temperature SCR have been widely researched [9-11]. MnO_X-based catalysts are specifically gaining much attention in recent years because of the high oxidation states and characteristic crystal structure [4]. Kang et al. reported NO conversions above 95% between 75 and 175 ºC with MnO_X supported over Al_2O_3 and CeO_2 [12], while Li et al. achieved total NO conversion between 150 and 200 ºC using TiO_2 as support [13]. The same way, their high efficiency in reduction/oxidation cycles and excellent oxygen migration ability are positive for the application of this type of catalysts in the oxidation of chlorinated organic compounds [14].

CeO_2 has been widely studied for its great redox properties and high oxygen mobility related to oxygen vacancies [3,7,15]. These are properties that benefit the faster oxidation of NO to NO_2 and chlorinated organic compound, involved in fast SCR and catalytic oxidation, respectively. Therefore, the addition of CeO_2 to MnO_X-based catalysts may improve the catalytic performance in the

simultaneous abatement of NO_X and PCDD/Fs. The enhancement of catalytic activity in NO reduction has been corroborated by several works. Qi et al. reported NO conversion of 95% at 150 ºC with MnO_X-CeO_2 mixed oxide catalysts [16]. Similar results where showed by Shen et al. in MnO_X/CeO_2 supported catalyst between 120 and 220 ºC [17]. The same way, the MnO_X-CeO_2 formulation leads to the catalytic oxidation of chlorobenzene above 250 ºC [18,19] and o-xylene above 220 ºC [20].

It has been reported that physicochemical properties and catalytic performance depend on preparation methods [21,22]. Regarding to literature, several routes have been used for the preparation of MnO_X-CeO_2 catalysts, such as co-precipitation [23-25], sol-gel [26,27], impregnation [17], modified co-precipitation [28] and redox precipitation [8,20]. Unfortunately, no agreement about what preparation method is the most suitable for the simultaneous abatement of NO_X and PCDD/Fs is found in the literature. This is due to the small number of works focused on the elimination of both pollutants simultaneously, rather than independently.

In this work, catalysts based on Mn and Ce oxides were prepared by two methods, characterized by different techniques and tested in the simultaneous abatement of NO and o-DCB, through NH_3-SCR and catalytic oxidation, respectively. The catalytic test was carried out in conditions close to those used in MSW incineration plants. Therefore, the goal of this work is to evaluate the influence of preparation method in physicochemical properties and catalytic performance of the catalysts, in order to conclude the optimum preparation method and composition.

2. EXPERIMENTAL

2.1. Catalysts preparation

Two series of catalysts based on Mn and Ce oxides were prepared to different metal contents by co-precipitation and impregnation, in order to obtain solids with different properties. The experimental procedure followed in each preparation method is explained in detail in the following.

2.1.1. Co-precipitation method

The necessary amount of a solution of $Mn(NO_3)_2 \cdot 4H_2O$ in distilled water (0.55 M Mn) and/or a solution of $Ce(NO_3)_3 \cdot 6H_2O$ in distilled water (0.35 M Ce) were mixed at room temperature under magnetic stirring and co-precipitated by dropwise addition of a 1.3 M solution of NH_2COONH_4 until the solution reached pH = 9. The resulting suspension was aged during 2 h, then filtered and washed with distilled water. The obtained solid was dried at 110 ºC for 12 h and calcined at 500 ºC for 3 h.

With this procedure, solids with a bulk homogeneous composition of the oxides are obtained, in which Mn and Ce can belong to a common oxide structure, and/or be segregated in structures characteristic of their typical oxides. In order to carry out the catalytic reactions in the absence of mass transfer limitations and with low pressure drop, the catalysts were pelletized, crushed and sieved to 0.3-0.5 mm.

Seven catalysts were prepared by this procedure, from pure CeO_2 to pure MnO_X, with five intermediate compositions, and named: 0Mn-100Ce (pure CeO_2), 15Mn-85Ce, 50Mn-50Ce, 80Mn-20Ce, 85Mn-15Ce, 90Mn-10Ce and 100Mn-0Ce (pure MnO_X); where the numbers indicate the molar percentage of each oxide in the samples.

2.1.2. Impregnation method

CeO_2 support was prepared by thermal decomposition of $Ce(NO_3)_3 \cdot 6H_2O$ at 550 ºC for 3 h. Then, an aqueous solution with the proper amount of $Mn(NO_3)_2 \cdot 4H_2O$ was used to impregnate this support. The precursor solution and the support (2 mL/g) were mixed in a rotary evaporator, where the resulting slurry was kept in contact in continuous stirring for 1 h to improve homogeneity. Then, the solvent was evaporated by increasing the temperature to 40 ºC in vacuum conditions. Finally, the solid was dried at 110 ºC for 12 h, calcined at 500 ºC for 3 h and pelletized, crushed and sieved to 0.3-0.5 mm.

With this procedure, supported catalysts are obtained, in which the active phase, MnO_X, is located on the surface of the CeO_2 support to different surface coverage. Six catalysts were prepared by this procedure, with Mn content ranging from 0 to 8 wt.%, and named: $0Mn/CeO_2$ (the support, pure CeO_2), $1Mn/CeO_2$, $2Mn/CeO_2$, $3Mn/CeO_2$, $5Mn/CeO_2$ and $8Mn/CeO_2$. In order to complete the series, an additional sample of pure manganese oxide (named as MnO_X) was prepared by thermal decomposition of $Mn(NO_3)_2 \cdot 4H_2O$ at 500 ºC for 3 h.

2.1.3. Comparison between preparation methods

Taking into account both preparation methods, global composition of both catalyst series is very different. However, comparison can be made in terms of surface coverage of MnO_X, taking into account that catalysis is a surface phenomenon. Both series of catalysts have been prepared with the idea to cover the whole range of surface coverage, from 0 (pure CeO_2) to 1 (pure MnO_X).

In co-precipitation catalysts, molar composition gives a direct estimation of theoretical relative surface coverage, and that is the reason why composition of these catalysts is given as molar percentage of the oxides all over the paper.

In impregnation catalysts, MnO_X is only located at the surface. Thus, Mn content remains much smaller for similar surface coverage. In these catalysts, compositions are usually given as weight percentage of the active metal, and that is the reason why composition of these catalysts is given as wt.% Mn all over the paper. Taking into account the cross sectional area of MnO_X [29], the specific surface area of the support (CeO_2) and the probable multilayer deposition at high coverage, the $8Mn/CeO_2$ sample should very nearly approach total MnO_X surface coverage.

2.2. Catalyst characterization

2.2.1. XRD analysis

X-ray diffraction (XRD) was conducted on a Philips PW 1710 X-ray diffractometer with Cu Kα radiation (λ = 1.5406 Å) and Ni filter. The finely ground samples were scanned between 10° and 100° (2θ) with a 2θ step size of 0.026° and counting time of 528 s. Crystal phases were identified by comparison with JCPDS (Joint Committee on Powder Diffraction Standards) database cards.

2.2.2. Textural properties

Textural properties were evaluated by N_2 adsorption–desorption isotherms at −196 ºC, in a Micromeritics TRISTAR II 3020. Specific surface areas of the catalysts were calculated by the standard BET procedure, using adsorption branch data in the relative equilibrium pressure range of 0.03-0.3. Pore average

size and distribution were calculated using the BJH method from the desorption branch. The samples (15-20 mg) were previously degassed under nitrogen flow at 350 ºC for 4 h.

2.2.3. Raman spectroscopy

Raman spectroscopy was performed in a Renishaw System 1000 Raman spectrometer. A 514 nm solid-state laser was used as excitation line with a power on the sample of 1 mW. All measurements were carried out at room temperature.

2.2.4. H_2-TPR analysis

Temperature programmed reduction with H_2 (H_2-TPR) was used to evaluate the redox properties of the catalysts. The experiments were performed on a Micromeritics AutoChem 2920 instrument. First of all, the samples (15-20 mg) were pre-treated under 50 cm^3/min of 5% O_2/He mixture at 500 ºC for 45 min and cooled down to 40 ºC in helium. Then, the samples were heated from 40 to 950 ºC with a rate of 10 ºC/min under 50 cm^3/min of 5% H_2/Ar. The water produced by reduction was trapped in a cold trap, and the consumption of H_2 was continuously monitored with a TCD. Total H_2 consumption was calculated from time-integration of TCD signal.

2.2.5. XPS characterization

X-ray Photoelectron Spectroscopy (XPS) was performed on an Al Kα (1486.6 eV) SPECS system (Berlin, Germany) equipped with 1D-150 Phoibos DLD analyzer and monochromatic radiation source. Detailed analysis of the elements (energy step 0.1 eV, dwell time 0.1 s, pass energy 30 eV) was performed with an electron exit angle of 90°. The spectra were fitted by

CasaXPS 2.3.16 software, modeling the Gauss-Lorentzian contributions after background subtraction (Shirley).

2.2.6. NH_3-TPD analysis

Catalysts surface acidity was measured by temperature programmed desorption of ammonia (NH_3-TPD) carried out on a Micromeritics AutoChem 2920 instrument. Before adsorption, all samples (15-20 mg) were pretreated under 50 cm^3/min of 5% O_2/He mixture at 500 ºC for 45 min and cooled down to 40 ºC in helium. The adsorption step was performed by 130 cm^3/min of 1% NH_3/He mixture gas at 40 ºC during 60 min. Then, the samples were exposed to 130 cm^3/min of helium for 60 min in order to remove physisorbed NH_3 from the surface. TPD experiments started from 40 to 450 ºC with a heating rate of 10 ºC/min and helium as carrier. NH_3 desorbed from the catalysts was continuously monitored with a TCD. Total acidity was calculated by time-integration of TCD signal.

2.2.7. Elemental analysis

Elemental analyses of deactivated catalysts (after stability tests) were conducted by XRF and EDS, in the case of chlorine, and EDS for carbon. XRF analysis was conducted in a wavelength dispersive X-ray fluorescence sequential spectrometer (WDXRF, PANalytical, AXIOS model) with Rh tube. EDS analysis was performed in a Carl Zeiss EVO 40 equipped with an EDS detector (Oxford Instrument X-Max). The measurements were made at 20 kV of voltage, 100-400 pA of current and at 10 nm approximately.

2.3. Experimental reaction set-up and catalytic tests

The experimental reaction set-up is shown in Fig. 1. The gas mixture was prepared to simulate the actual MSW incinerator combustion gases. Due to the high toxicity and operational problems arising from working with PCDD/Fs, most researchers usually use model compounds, less toxic and with similar structure. Thus, in this work, o-DCB has been used as the alternative to PCDD/Fs [30,31]. The composition of catalytic reactor feed was: O_2 (10%), NO (300 ppm), NH_3 (300 ppm), o-DCB (100 ppm) and Ar to balance. Gas flows were regulated by gas mass flow controllers (Bronkhorst® High-Tech F-201CV), whereas o-DCB and water liquid stream was dosed by a Bronkhorst® High-Tech μ-Flow L01-AAA-99-0-20S mass flow controller. In order to avoid the complete evaporation of the liquid component and favor the homogenous mixture with the gas stream, a controlled-evaporator-mixed (Bronkhorst® High-Tech W-102A-111-K) was used. Moreover, all pipes were hot, avoiding gas adsorption and condensation. The catalytic bed was formed by 1.5 g of particulate catalyst (0.3-0.5 mm) mixed with inert quartz (0.5-0.8 mm) in order to fill a bed volume of 3 cm^3, resulting in a GHSV value of 40,000 h^{-1}. The fixed catalytic bed was inside a U-shaped tubular quartz reactor (13.6 mm internal diameter), which was heated into a convective-flow oven.

Fig. 1

An on-line gas chromatograph (Agilent Technologies 7890A) equipped with a HP-VOC capillary column and a 5975C mass selective detector was used to quantify o-DCB concentration in the reactor inlet and outlet streams and also to detect possible chlorinated byproduct compounds. Furthermore, NO, NO_2 and NH_3 were continuously measured by ultra-violet (ABB, Limas 21), whereas CO_2, CO and N_2O were analyzed by infrared (ABB, Uras 26). During reaction, NH_3 is

not measured due to the interference between o-DCB and the Limas 21 analyzer. Because of this, NH_3 was only measured before reaction, in order to verify its inlet concentration.

Before each experiment, the catalyst was pretreated with pure argon flow (2 L_N/min) at 200 ºC for 2 h in order to remove the compounds adsorbed on the surface. The catalytic activity was measured by light-off curves at a pressure of 1.5 atm by feeding a constant total flow of 2 L_N/min and increasing the temperature from 100 to 450 ºC with a constant heating rate of 1.5 ºC/min. Stability tests were carried out at 300 ºC, keeping this temperature constant during 24 hours.

NO and o-DCB conversions were calculated from Ec. (1) and (2), respectively, as:

$$X_{NO} = \frac{NO_{in} - NO_{out}}{NO_{in}} \cdot 100 \quad (3)$$

$$X_{oDCB} = \frac{oDCB_{in} - oDCB_{out}}{oDCB_{in}} \cdot 100 \quad (4)$$

and selectivity to CO_2 and CO with:

$$S_{CO_2} = \frac{CO_2}{6 \cdot (oDCB_{in} - oDCB_{out})} \cdot 100 \quad (5)$$

$$S_{CO} = \frac{CO}{6 \cdot (oDCB_{in} - oDCB_{out})} \cdot 100 \quad (6)$$

3. RESULTS

3.1. Catalysts characterization

3.1.1. XRD analysis

Fig. 2A and 2B show the XRD patterns of the catalysts prepared by co-precipitation and impregnation, respectively. CeO_2 in co-precipitation and impregnation series, 0Mn-100Ce and 0Mn/CeO_2, show the same diffraction peaks of cerionite, characteristic of cubic fluorite structure (JCPDS, 00-004-0593). On the other hand, manganese oxide of co-precipitation and impregnation series, 100Mn-0Ce and MnO_X, present clearly different diffraction patterns. Diffraction peaks of 100Mn-0Ce are associated to α-Mn_2O_3 phase (JCPDS, 01-078-030), whereas those of MnO_X are related to both α-Mn_2O_3 and β-MnO_2 (JCPDS, 00-050-0866) phases.

In the co-precipitation series, peaks associated to fluorite structure show a shift to higher Bragg angles with increasing Mn content, which is associated to the contraction and distortion of the fluorite structure caused by Mn insertion forming a solid solution. Ionic radii of Mn^{4+} (0.53 Å), Mn^{3+} (0.65 Å) and Mn^{2+} (0.83 Å) are smaller than that of Ce^{4+} (1.01 Å), which produces the lattice parameter modification (decrease) with increasing Mn content shown in Table 1 [32]. Additional evidence for the formation of a solid solution is the observed broadening of the diffraction peaks of fluorite phase, associated to the decrease of fluorite crystal size, with increasing Mn content (Table 1), which indicates a loss of crystallinity due to the structural defects caused by Mn insertion. Above 80 mol.% MnO_X, additional sharp diffraction peaks associated to Mn_2O_3 can be observed in Fig. 2A, caused by segregation from the fluorite structure because

of saturation [33], in agreement with the increase in Mn_2O_3 crystal size with Mn content (Table 1).

In the impregnation series, only peaks associated to fluorite structure can be found up to 5 wt.% Mn. The absence of diffraction peaks associated to MnO_X indicates that Mn species are highly dispersed on the CeO_2 surface. However, a diffraction peak associated to MnO_2 appears at 37.6° in the 8Mn/CeO_2 sample, supported catalyst with the highest Mn content, which indicates that Mn tends to form crystal aggregates of MnO_2 over the support at high coverage. In this case, no insertion of Mn on CeO_2 lattice is observed, as lattice parameter in Table 1 remains constant with increasing Mn content.

Thus, co-precipitation catalysts above 80 mol.% MnO_X consist of a MnO_X-CeO_2 solid solution and Mn_2O_3 crystals, so that Mn in high oxidation states coexist in different phases at high Mn content. In impregnation catalysts, on the other hand, no solid solution is observed and Mn in the form of MnO_2 is only in contact with surface CeO_2.

Table 1

Fig. 2

3.1.2. Textural properties

BET surface area and pore volume of catalysts were measured by N_2 physisorption and the results are listed in Table 1. In general, surface area and pore volume of co-precipitation catalysts are higher than those of impregnation catalysts.

In the co-precipitation catalysts, surface area of the intermediate compositions is higher than that of the pure oxides (0Mn-100Ce and 100Mn-0Ce) and pore volume notably increases with Mn content. In impregnation catalysts, on the

other hand, increasing Mn content produces a decrease in surface area, and a maximum pore volume around 2Mn/CeO_2. The decrease in pore volume above 3 wt.% Mn is probably associated to the formation of larger particles of MnO_X blocking the CeO_2 porous structure.

These results indicate that interaction of MnO_X and CeO_2 in co-precipitation catalysts, observed in XRD, generates structural defects in the bulk leading to higher exposure of catalyst surface and pores compared to impregnation catalysts. This feature probably contributes to the enhancement of catalytic performance by the increase of reaction sites.

3.1.3. Raman spectroscopy

Raman spectroscopy is useful to obtain information about alterations into the structure of the catalysts through the investigation of metal-oxygen vibrations. Fig. 3A and 3B show Raman spectra of catalysts prepared by co-precipitation and impregnation, respectively.

Spectra of pure CeO_2 samples, 0Mn-100Ce and 0Mn/CeO_2, exhibit an intense band at 460 cm^{-1}, associated to F_{2g} vibration mode [34,35]. This band is related to symmetrical stretching vibration of the atoms belonging to the structure around Ce^{4+} [36]; so, it will be affected by alteration in the environment of sublattice oxygen. The F_{2g} vibration mode is also detected in all catalysts containing both MnO_X and CeO_2.

In the co-precipitation series, increasing Mn content produces a shift of F_{2g} band to lower wavenumber, from 460 cm^{-1} in 0Mn-100Ce down to 446 cm^{-1} in 80Mn-20Ce catalyst. This result proves the modification of the CeO_2 structure by the incorporation of Mn, and corroborates the solid solution formation. Together with F_{2g} displacement, the increase of Mn content promotes the appearance of

a band at 597 cm^{-1}, associated to oxygen vacancies [36]. Oxygen vacancies appear to compensate the negative charges generated by the incorporation of a doping cation with different nature and oxidation state [25]. Thus, the band at 597 cm^{-1} is another evidence of the formation of a solid solution in this series. Above 80 mol.% MnO_X, an additional band appears at 635 cm^{-1} overlapping with the band associated to oxygen vacancies. This band is associated to MnO_X and increases its intensity with Mn content, whereas F_{2g} gradually decreases, which confirms the change of lattice parameter observed by XRD [37]. Pure MnO_X (100Mn-0Ce) shows bands at 693, 640 and 306 cm^{-1} associated to vibrational modes v_7, v_6 and v_2 of α-Mn_2O_3 [38] in agreement with the results of XRD.

In the impregnation series, the position of F_{2g} band does not change with increasing Mn content. Besides, no clear evidence of Mn-O stretching modes is observed in the spectra of the supported samples, not even in 8Mn/CeO_2, which denotes the good dispersion of Mn on the support surface in this series. Concerning pure MnO_X, bands at 760, 662, 553 and 317 cm^{-1} associated to vibrational modes v_8, v_6, v_5 and v_2 of β-MnO_2 can be observed, in accordance with the results of XRD.

Fig. 3

3.1.4. H_2-TPR analysis

Redox properties were investigated by H_2-TPR. Fig. 4A and 4B show the H_2 consumption curves of catalysts prepared by co-precipitation and impregnation, respectively. TPR profiles of CeO_2 in both series, 0Mn-100Ce and 0Mn/CeO_2 samples, are very similar. They show two broad peaks located around 430 and 830 ºC, related to surface and bulk CeO_2 reduction, respectively [15]. Redox

properties are enhanced to different extent by the presence of Mn in the catalysts with respect to those of CeO_2. This enhancement can be associated to structural defects generated by surface interaction in impregnation catalysts.

In the co-precipitation series, a reduction peak around 100 ºC can be observed in the catalysts up to 50 mol.% MnO_X, associated to surface isolated Mn ions "embedded" into CeO_2 lattice [19,39]. Increasing Mn content, two strongly overlapped peaks at 266 and 300 ºC and an additional peak at 400 ºC appear. Pure manganese oxide, 100Mn-0Ce, presents two reduction peaks at 293 and 435 ºC, which fit very well with pure Mn_2O_3 reduction profile in the literature [40,41], in accordance with XRD results, as time-integration of the TPR profile reveals that H_2 consumed in the first peak is half that in the second, which agrees with the stoichiometry of two reduction steps: the first peak related to the reduction of Mn_2O_3 to Mn_3O_4 and the second to the reduction of Mn_3O_4 to MnO.

In the impregnation series, two clear reduction peaks around 320 and 410 ºC associated to MnO_X reduction can be observed. In addition, surface CeO_2 reduction is also present in the range 200-400 ºC, although it is difficult to distinguish. Pure manganese oxide sample, MnO_X, also shows two reduction peaks, but shifted to higher temperatures and strongly overlapped (compared to 100Mn-0Ce), at 406 and 532 ºC. Similar TPR profile is reported by Shen et al., who associated the first reduction peak to the reduction or MnO_2 and Mn_2O_3 to Mn_3O_4 and the second to the reduction of Mn_3O_4 to MnO [24].

Several works in the literature agree that MnO_2 reduction in catalysts is practically indistinguishable from that of Mn_2O_3. Thus, many authors associate H_2 consumption at low temperature (around 300 ºC) to the reduction of MnO_2/Mn_2O_3 to Mn_3O_4, and H_2 consumption at intermediate temperature

(around 400 ºC) to the reduction of Mn_3O_4 to MnO and surface CeO_2 [24,32,42], when explaining TPR profiles. However, the appearance of two overlapped peaks at low temperature in co-precipitation catalysts brings to light the reduction of different phases in high oxidation state: the reduction of Mn ions embedded into cerium oxide lattice and the reduction of MnO_X crystals well-dispersed over the catalysts. The high interaction between both phases is responsible for the strong overlapping or these two peaks in the TPR profile. It should be noted that the first reduction peak, located at 266 ºC, increases with Mn content. The same way, XRD results above showed that high Mn content favored the presence of bigger Mn_2O_3 crystals in the catalysts. As a result, we propose that the first reduction peak is associated to reduction of MnO_X crystals, which would have better accessibility to H_2 because they are segregated from the solid solution. On the other hand, the peak around 300 ºC is related to reduction of Mn incorporated to the CeO_2 structure. Therefore, the results obtained in TPR are in accordance with those obtained through other techniques, supporting the formation of the solid solution in the co-precipitation series.

In these catalysts, several species are observed depending on Mn content. Low Mn contents favor the presence of isolated Mn located into the CeO_2 structure, whereas high Mn content promotes its segregation from the solid solution, creating crystalline aggregates.

H_2 consumption in TPR has been summarized in Table 2. In the co-precipitation series, H_2 consumption increases with Mn content. In the impregnation series, this is also truth in general, but H_2 consumption of the support ($0Mn/CeO_2$) is somewhat higher than that of the lowest Mn content sample ($1Mn/CeO_2$). The

results of H_2 consumption have been used to estimate average oxidation state of Mn in the catalysts, assuming MnO as the final reduction state of Mn (and similar reduction of CeO_2), and these results have been also added to Table 2, together with the proportion of Mn^{3+} and Mn^{4+}.

In the co-precipitation series, increasing Mn content produces a decrease in average oxidation state of Mn in the catalyst. Thus, at low Mn content, 15Mn-85Ce sample, the calculated average Mn oxidation state is 4. For this catalyst, the results of characterization above showed that all Mn was incorporated to CeO_2 structure; consequently, Mn^{4+} is the main species promoted when Mn is inside CeO_2 structure. At high Mn content, above 80 mol.% MnO_X, average Mn oxidation state decreases to 3.2-3.3, which suggests a coexistence of Mn^{4+} and Mn^{3+} species. The appearance of Mn^{3+} is favoured by the formation of Mn_2O_3 crystals. Pure manganese oxide, 100Mn-0Ce sample, in fact, shows an average Mn oxidation state around 3 in good agreement with XRD results, where only peaks associated to Mn_2O_3 were observed.

In the impregnation series, error in the estimation can be important below 3 wt.% Mn. However, average Mn oxidation state is above 3.5 in 5Mn/CeO_2 and 8Mn/CeO_2 samples. This fact suggests that higher Mn coverage leads to agglomeration in bigger crystals (as concluded by XRD) in which Mn^{4+}, in the form of MnO_2, is the main oxidation state. MnO_X sample in this series shows an average Mn oxidation state around 3.1, in line with the mixture of Mn_2O_3 and MnO_2 observed in XRD.

Table 2

Fig. 4

3.1.5. XPS characterization

Surface composition and surface oxidation states of the elements in the catalysts were studied by XPS. Fig. 5 shows Ce 3d, Mn 2p and O 1s spectra of co-precipitation (Fig. 5A, 5C and 5E) and impregnation (Fig. 5B, 5D and 5F) catalysts. All binding energies are referenced to elemental carbon (C 1s) spectrum at 284.5 eV.

Ce 3d spectra (Fig. 5A and 5B) have only been analyzed by their 5/2 spin orbit doublet, because of the overlapping of Ce and Auger Mn line at high Mn content. Ce 3d 5/2 is deconvolved in 5 peaks with V notation for the assignment to Ce^{3+} and Ce^{4+}. Thus, V, V^{II} and V^{III} peaks are associated to Ce^{4+}, and V^{0} and V^{I} peaks to Ce^{3+} [43,44]. A clear presence of surface Ce^{4+} and Ce^{3+} is observed in all samples. In this way, surface proportion of both species in the catalysts was calculated by XPS integration, and the values are summarized in Table 3. Similar values are observed for both co-precipitation and impregnation catalysts, although with slightly higher proportion of Ce^{3+} surface species in the impregnation series. Ce^{3+} species are commonly associated to surface oxygen vacancies [34,45].

Mn 2p spectra of the catalysts (Fig. 5C and 5D) show a spin-orbit doublet Mn 2p 3/2 and Mn 2p 1/2, which were deconvolved in three components related to Mn^{3+}, Mn^{4+} and a satellite [46,47], located around 641.0, 642.5 and 646.7 eV, respectively. The satellite peak intensity was weak in all samples compared to Mn^{3+} and Mn^{4+}. The presence of Mn^{3+} and Mn^{4+} is in accordance with the results obtained by XRD and TPR, in which both types of Mn species were detected. Surface proportion of both Mn species in the samples was calculated by XPS integration, and the values are also summarized in Table 3.

In co-precipitation catalysts, all samples show similar oxidation state of Mn in the surface, around 3.5, which suggests that proportion of surface Mn^{3+} and Mn^{4+} is similar in all samples, and different from that in the bulk (obtained by TPR, Table 2.). Apparently, surface and bulk proportion of Mn^{3+} and Mn^{4+} would be similar in 50Mn-50Ce sample, the surface would be enriched in Mn^{3+} below 50 mol.% MnO_X, and the surface would be enriched in Mn^{4+} above 50 mol.% MnO_X.

On the other hand, surface proportion of Mn^{3+} and Mn^{4+} in impregnation catalysts is also the same in all samples, and similar to that of the co-precipitation series, the proportion of Mn^{3+} being higher in the surface than the bulk, in general.

The differences between surface and bulk proportions of Mn^{3+} and Mn^{4+} with preparation method at high Mn content are probably related to different MnO_X crystals promoted by each preparation method.

Fig. 5E and 5F show the O 1s spectra of catalyst samples. In the impregnation series, the high Ce content produces a decrease in conductivity of the samples, which causes unsuitable spectra for deconvolution. For this reason, only O 1s of co-precipitated catalysts was deconvolved in three peaks. Each peak is associated to different surface oxygen species.

In the co-precipitation series, pure CeO_2, 0Mn-100Ce sample, the peak at 529.5 eV (O^I) is associated to lattice oxygen. This peak is shifted to lower binding energy in Mn-containing catalysts, due to the formation of the solid solution. Although O 1s profile was not deconvolved in impregnation catalysts, a clear shift to lower binding energies is also observed in the peak located around

529.8 eV in the Mn-containing catalysts with respect to 0Mn/CeO_2, as a consequence of the interaction between Mn and the support.

The intermediate binding energy peak, located around 531.2 eV (O^{II}), is related to adsorbed oxygen on the surface, whereas the high binding energy peak, at 533.2 eV (O^{III}), is associated to molecular water and carbonate species adsorbed on the catalysts [24,48]. Yao et al. proposed a process of oxygen storage/release in which adsorbed oxygen is involved in the reduction of CeO_2 to Ce_2O_3 to form oxygen vacancies [21]. In this way, relative O^{II} concentration may give an approximation of the amount of oxygen vacancies present in the surface of the catalysts. Thus, $O^{II}/(O^{I} + O^{II} + O^{III})$ ratio has been calculated for the co-precipitation catalysts and summarized in Table 3. We can see that increasing Mn content promotes higher relative O^{II} concentration, which evidences an increase of the amount of oxygen active species involved in the formation of oxygen vacancies, useful for the activation of reactants of SCR and oxidation reactions.

Table 3

Fig. 5

3.1.6. NH_3-TPD analysis

Acid properties were studied by NH_3-TPD experiments. NH_3 desorption profiles of the catalysts prepared by co-precipitation and impregnation are shown in Fig. 6A and 6B, respectively. Acid properties are involved in the adsorption and activation of the compounds used in both SCR and oxidation reactions. The position of the NH_3 desorption peaks is associated to the strength of the acid sites. Thus, peaks located at low temperature will be related to NH_3 desorbed from weak acid sites, while the peaks located at high temperature are attributed

to NH_3 desorption from strong acid sites [21,49]. The amount of the acid sites is related to the integrated area of the peaks.

NH_3 desorption profiles of pure CeO_2 in both series, 0Mn-100Ce and 0Mn/CeO_2, show a peak around 110 ºC, associated to weak acidity, and a shoulder at 220 ºC, related to strong acidity.

In the co-precipitation series, low Mn content promotes strong acidity with respect to 0Mn-100Ce (an increase of the intensity of the peak at 220 ºC). Moreover, an increase of NH_3 desorption at temperatures around 160 ºC, broadening the low-temperature desorption peak, is observed above 80 mol.% MnO_X. This fact evidences that high Mn content produces an increase of weak acidity, probably associated to the Mn_2O_3 phase. Pure manganese oxide, 100Mn-0Ce sample, presents two desorption peaks at 100 and 187 ºC. Compared to the mixed oxides, peaks in 100Mn-0Ce are shifted to lower temperature, which indicates that the presence of Ce promotes stronger interaction between NH_3 and the catalysts and, thus, stronger acid sites, which may be caused by the enhancement of redox properties observed by TPR.

In the impregnation series, the presence of Mn contributes to increase the strong acidity because of the appearance of a peak at 220 ºC. No clear desorption peaks were observed for MnO_X sample, probably because of the low surface area of that sample (see Table 1).

Quantitative results for acidity, calculated by time-integration of the TCD signal, are summarized in Table 2. Comparison between the two catalyst series reveals that co-precipitation catalysts show higher acidity than impregnation catalysts, which may be associated to the higher interaction between Mn and Ce through the solid solution, taking into account that acidity is also higher per

unit surface area (see Table 2). Moreover, different correlation between weak and strong acidity has been found depending on preparation method and composition.

In the impregnation series, higher Mn content promotes strong acidity in detriment of weak acidity. However, above 5 wt.% Mn (composition from which MnO_X crystals were detected by XRD) a decrease of both types of acidity is observed. Although this effect could partially be associated to lower surface area (see Table 1), the calculated acidity per unit area in Table 2 remains lower. Therefore, these results suggest that highly-disperse Mn is the species promoting catalyst acidity, and MnO_2 is detrimental for both weak and strong acidity.

Fig. 6

3.2. Catalytic performance

3.2.1. Catalytic activity

Fig. 7 shows simultaneous NO SCR and o-DCB oxidation catalytic activity of co-precipitation (Fig. 7A and 7B) and impregnation (Fig. 7C and 7D) catalysts. Co-precipitation catalysts are clearly more active than impregnation catalysts.

Concerning NO SCR, pure CeO_2 samples, 0Mn-100Ce and 0Mn/CeO_2, are active in SCR from 250 ºC, reaching the maximum NO conversion of 85% at 350 ºC, approximately.

The incorporation of Mn in co-precipitation catalysts (Fig. 7A) improves catalytic activity in SCR. At low Mn content (15Mn-85Ce catalyst) NO conversion profile is similar to that obtained with impregnation catalysts (Fig. 7C), although it does not enhance the one obtained with 100Mn-0Ce. Mn content above 50 mol.%

MnO_X leads to NO conversion above 95% in the 100-200 ºC temperature range. NO conversion decays in the high-temperature range because of the appearance of side reactions (NH_3 oxidation), which consume the reactants involved in SCR.

In the impregnation catalysts (Fig. 7C), incorporation of Mn promotes an increase of NO conversion up to 70% at temperatures above 150 ºC. However, the further increase of temperature produces a decay of NO conversion, which increases again from 50 to 75% in the medium temperature range. Temperatures above 350 ºC produce a drastic drop of NO conversion in all catalysts. No great differences of NO conversion profiles have been observed among catalysts with MnO_X and CeO_2 in their composition, although the catalyst with the lowest Mn content favors slightly higher NO conversion at low temperature.

Comparing between both series, the temperature at which NO conversion starts to decrease is higher in impregnation catalysts and pure CeO_2 samples than in co-precipitation catalysts. This result suggests that Mn improves the oxidation properties of the catalysts, shifting NH_3 oxidation to lower temperatures.

Fig. 7

Regarding oxidation reaction, Fig. 7B and 7D, addition of MnO_X to CeO_2 promotes catalytic activity in both series of catalysts. o-DCB conversion profiles are similar in all catalysts: they show a maximum at low temperatures from which o-DCB conversion decays, and then strongly increases with temperature. o-DCB conversion values at low and high temperature depend on Mn content and preparation method.

In the co-precipitation series, 15Mn-85Ce sample showed similar results than impregnation catalysts (Fig. 7D), although with higher o-DCB conversion values (85 and 99% at 280 and 450 ºC, respectively). The increase of Mn content shifts o-DCB conversion profiles to lower temperatures. Thus, catalysts above 80 mol.% MnO_X present the best activity, with o-DCB conversions above 85% at 200 ºC, and total conversion at temperatures above 325ºC.

In the impregnation series, higher Mn loading increases catalytic activity, 5Mn/CeO_2 and 8Mn/CeO_2 being the best impregnation catalysts, with o-DCB conversion of 60 and 90% at 280 and 450 ºC, respectively. The similar decay of o-DCB conversion at medium temperature in both co-precipitation and impregnation catalysts should be noted, which could be attributed to oxidation occurring through different pathways depending on temperature.

Summarizing, catalysts with both MnO_X and CeO_2 in their composition, especially those with high Mn content, showed better catalytic performance than pure oxides in the simultaneous removal of NO and o-DCB. These results reveal that, although Mn species are the main contribution to catalytic activity, a little amount of Ce becomes important to reach higher conversion of o-DCB and total conversion of NO at low temperature. Moreover, catalysts prepared by co-precipitation showed the best catalytic activity, with higher NO and o-DCB conversion at lower temperatures than impregnation catalysts. According to characterization, higher interaction between Mn and Ce was evidenced in co-precipitation catalysts, which bring to the light the relevance of the interaction between both metals as the key factor to improve catalytic activity in NO reduction and o-DCB oxidation.

Regarding to catalytic composition, co-precipitation catalysts above 80 mol.% MnO_X were found to present the best catalytic activity, leading to conversions above 80% of both NO and o-DCB in the temperature range of 180-300 ºC. In these catalysts, XRD results showed that they were not only composed by the solid solution of the oxides, but also by segregated Mn_2O_3 crystal aggregates. Moreover, TPR results showed that Mn tends to be as Mn^{4+} when inside CeO_2 structure, while as Mn^{3+} in Mn_2O_3 crystal aggregates. As a consequence, the synergy of both crystal phases provides Mn in different oxidation states, which is responsible for the great catalytic performances of high Mn content co-precipitation catalysts. This conclusion is in accordance with Dai et al., who proposed that Mn species in the interface between MnO_X and the solid solution and their neighbor lattice oxygen are the best active sites [48].

3.2.2. Analysis of by-products

In SCR, N_2O and NO_2 were found to be the main by-products. The production profiles of both compounds are shown in Fig. 8 for co-precipitation (Fig. 8A and 8B) and impregnation (Fig. 8C and 8D) catalysts, respectively. In pure CeO_2 samples of both series, 0Mn-100Ce and 0Mn/CeO_2, N_2O production is below 30 ppm in all temperature range. However, the addition of Mn, even in samples with the lowest Mn content, causes a remarkable increase of N_2O concentration in both co-precipitation and impregnation catalysts. Some works propose that N_2O formation is related to well-ordered MnO_X due to the presence of highly-reactive oxygen [28,50], while other authors propose that N_2O is associated to Mn content in the catalysts (independently of structure and order) at high temperature [51]. In this work, N_2O was found in all Mn-containing catalysts, with or without MnO_X crystals, and at temperatures above 150 ºC. Therefore,

these results suggest that N_2O formation is largely associated to catalytic properties provided by Mn and not by its content or structure. In this regard, TPD experiments showed that the incorporation of Mn greatly increased the acid properties of the catalysts. Acid properties are strongly related to reactants oxidation on the catalyst surface; so, they could also be related to N_2O formation through the promotion of NH_3 oxidation.

Fig. 8

Regarding to N_2O production, similar N_2O profiles with two characteristic maxima are observed in co-precipitation and impregnation catalysts. In the case of impregnation catalysts, the two N_2O peaks are located at the same temperatures, 235 and 420 ºC, and the production is very similar, 140 and 123 ppm, respectively. For co-precipitation catalysts, N_2O production is higher than in impregnation catalysts in all temperature range. MnOx content above 50 mol.% produces a shift of N_2O production peaks from 245 and 421 ºC to 200 and 340 ºC, respectively. The fact that N_2O profiles are composed by two maxima may be associated to two chemical reactions, such as NH_3 oxidation and the non-selective reduction of NO, being involved in the formation of N_2O. The contribution of each reaction would depend on temperature.

Regarding to NO_2, this compound is formed at temperatures above 300 ºC, and its concentration continuously increases with temperature, which is in line with the results of Want et al. [52]. Pure CeO_2 in both series, 0Mn-100Ce and 0Mn/CeO_2, are the catalysts with the lowest NO_2 production. Mn-containing catalysts show a remarkable increase of NO_2 production, which slightly increases with Mn content in co-precipitation catalysts (around 300 ppm of NO_2 at 450 ºC, for catalysts above 80 mol.% MnO_X). Higher NO_2 production may be

associated to the more oxidizing properties of co-precipitation catalysts due to better oxygen mobility and higher acidity. It should be noted the NO_2 production at temperatures below 300 ºC in impregnation catalysts. The same result is observed with co-precipitation 15Mn-85Ce catalyst. These facts reveal that Mn highly dispersed on CeO_2 promoted the formation of low amounts of NO_2 at low temperatures.

CO_2 and CO selectivity was calculated in order to carry out the by-products analysis in oxidation reaction. Fig. 9 shows the selectivity towards CO_2 of co-precipitation (Fig. 8A and 8B) and impregnation (Fig. 8C and 8D) catalysts from 200 ºC (below this temperature, some catalysts presented very low o-DCB conversion). CO_2 selectivity fits very well with o-DCB conversion results (Fig. 7). An increase of CO_2 selectivity is observed with Mn content in both, co-precipitation and impregnation catalysts. Comparison between quantitative results obtained by the different preparation methods reveals that co-precipitation catalysts above 50 mol.% MnO_X promote, to a great extent, total oxidation of o-DCB, leading to CO_2 selectivity of 85 and 95% in the temperature ranges of 200-350 ºC and 350-450 ºC, respectively.

Fig. 9A and 9C show a drop in CO_2 selectivity at intermediate temperature. This drop is common in all samples containing both MnO_X and CeO_2, and coincides with the drop in o-DCB conversion (Fig. 7B and 7D). This fact may be associated to a promotion of partial oxidation, which would favor the appearance of oxidation products other than CO_2. CO was the main by-product from oxidation reaction and its selectivity is show in Fig. 9B and 9D. In impregnation catalysts, except for $1Mn/CeO_2$, all catalysts containing both MnO_X and CeO_2 show selectivity to CO below 15% in all temperature range. On

the other hand, co-precipitation catalysts promote selectivity to CO with Mn content at temperatures below 300 ºC. However, a drastic drop of selectivity to CO occurs at high temperature because of promotion of total oxidation of o-DCB. A slight increase in CO selectivity at intermediate temperatures, where CO_2 selectivity drops in both co-precipitation and impregnation catalysts with both MnO_X and CeO_2, should be noted. Moreover, the increase in CO selectivity is accompanied by the appearance of chlorinated by-products (Fig. 10). This fact corroborates that, under these conditions, o-DCB oxidation is promoted through partial oxidation, which has a negative effect in total oxidation.

Tetrachloroethylene and trichlorobenzene were the main chlorinated by-products identified in the temperature range of 275-420 ºC. The production of these compounds depends on Mn content. Thus, Fig. 10 shows that the formation of tetrachloroethylene in co-precipitation catalysts increases with Mn content, whereas trichlorobencene is promoted by high Ce contents. In the case of impregnation catalysts, trichlorobencene is the main by-product detected, because of the high Ce content, although traces of tetrachloroethylene are also detected in the impregnation catalysts with both MnO_X and CeO_2.

Fig. 10

Therefore, by-products formation and the slight increase of CO selectivity at intermediate temperature are in accordance with CO_2 selectivity decrease. This fact, and the decrease of o-DCB conversion in the same temperature range, suggests a change in o-DCB oxidation pathway through partial oxidation reactions. According to literature, nucleophilic and electrophilic substitution through C-Cl bond is usually considered as the initial step of o-DCB oxidation, because of the weakness of this bond [53]. However, at intermediate and high

temperature, C-H bond in o-DCB becomes weaker because of the oxidizing power provided by Mn. So o-DCB could be also broken through other bonds of the molecule. This fact would evidence the coexistence of two pathways at medium-high temperature. In the first pathway, o-DCB would be oxidized through C-Cl bond, whereas in the second pathway o-DCB would be oxidized through C-H bond, promoting the appearance of chlorinated by products.

The appearance of the second pathway occurs at different temperature depending on oxidizing power of the catalysts. In this sense, Fig. 10 shows that chlorinated by-products are formed at lower temperature in co-precipitation catalysts. Characterization experiments showed that these catalysts presented better redox and acid properties, which improve their oxidizing performance. These results would be the reason why the high-temperature mechanism, evidenced by the appearance of chlorinated by-products, appears at lower temperature in co-precipitation catalysts.

3.2.3. Stability tests

Deactivation is an important aspect in the reactions involving catalytic oxidation of VOCs. In order to analyze the influence of Mn content and preparation method in deactivation, co-precipitation and impregnation catalysts with different Mn contents were tested during 24 h in the simultaneous NO SCR and o-DCB oxidation at 300 ºC.

SCR results (Fig. 11A) show that NO conversion stabilized after 100 minutes in all catalysts. In co-precipitation catalysts, the trend in NO conversion differs depending on Mn content. In this way, the catalysts above 50 mol.% MnO_X show a decrease of NO conversion, so a clear deactivation of these catalysts occurs for SCR reaction. However, for 15Mn-85Ce, NO conversion increases

initially. Stationary NO conversion is slightly higher in the catalysts with lower Mn content, and NO conversions of 88, 85 and 81% were obtained for 15Mn-85Ce, 50Mn-50Ce and 85Mn-15Ce, respectively. On the other hand, impregnation catalysts show similar results with final NO conversions of 88, 86 and 86% for 2Mn/CeO_2, 5Mn/CeO_2 and 8Mn/CeO_2, respectively. In this case, no initial deactivation of the catalysts was observed, NO conversion increasing up to the final values, as in the lowest-Mn-content co-precipitation catalyst. Stability results are in accordance with those from light-off experiments.

Fig. 11C shows the evolution of by-products in SCR stability tests. NO_2 and N_2O concentration decreases in 85Mn-15Ce and 8Mn/CeO_2 catalysts in the first 100 minutes of reaction. The fact that by-products concentration decreases in both catalysts in spite of the different trend observed in NO conversion refutes that Mn content affects SCR pathway and the side reactions involved in this process.

Fig. 11

Regarding to o-DCB oxidation (Fig. 11B), a clear deactivation is observed in the first 5 hours both in co-precipitation and impregnation catalysts. After this time, o-DCB conversion remains constant around 13% in impregnation catalysts, whereas a smooth continuous decrease can be observed in co-precipitation catalysts, and o-DCB conversions of 70, 47 and 20% are obtained with 85Mn-15Ce, 50Mn-50Ce and 15Mn-85Ce, respectively, after 24 hours.

Concerning CO and CO_2 concentrations, Fig. 11D shows the evolution for 85Mn-15Ce and 8Mn/CeO_2 catalysts. The evolution of CO_2 is similar to that o-DCB conversion, with a strong initial decrease in both series. However, CO concentration increases, which indicates that deactivation affects not only o-

DCB conversion, but also selectivity. The increase of CO concentration is accompanied by the appearance of chlorinated by-products (not shown) in the co-precipitation series. In the impregnation series, however, chlorinated by-products are not observed, probably because of the small o-DCB conversion.

Summarizing, both co-precipitation and impregnation catalysts undergo significant deactivation in o-DCB oxidation. In SCR, co-precipitation catalysts above 50 mol.% MnO_X are slightly deactivated as well. According to literature, no evidences of deactivation have been reported in SCR in the absence of o-DCB [21,37]; thus, deactivation of the catalysts is probably strongly related to o-DCB oxidation. It is well known that oxidation of chlorinated compounds promotes deactivation effects in different types of catalysts at low temperature. Kan et al. associated the low-temperature deactivation of MnO_X-CeO_2 catalysts in the oxidation of chlorobenzene to the adsorption of Cl on the active sites [54]. On the other hand, Hetrick et al. evidenced a strong contribution of surface carbonaceous deposits in deactivation of VO_X/TiO_2 catalysts in m-DCB oxidation [55].

Table 4 summarizes chlorine and carbon content of used catalysts after stability tests. All catalysts show the presence of a high amount of chlorine and carbon on the surface, which corroborates the presence of the deactivating species proposed in the literature. Wang et al. proposed that deactivation by chlorine occurs mainly in the CeO_2 surface, and the temperature from which Cl_2 is formed as a by-product depends on Mn content, decreasing with increasing Mn content [19]. These results are in line with the lower surface chlorine detected at higher Mn content in both co-precipitation and impregnation catalysts in Table 4, which reveals that this deactivating species is eliminated more easily from the

surface when the amount of surface Mn is higher. However, no evidence of Cl_2 formation was observed in our experiments. This fact may be associated to the appearance of a white solid in the solid filter after the reactor, identified as ammonium chloride, which suggests that chlorine is removed by reaction with NH_3, one of the reactants in SCR. Easier removal of Cl at higher Mn content could be associated to weaker interaction of chlorine due to higher acidity and redox properties of the catalysts, taking into account the results of characterization.

Concerning carbon, co-precipitation catalysts present a surface carbon content decreasing with increasing Mn content. This result is probably associated to the improvement of oxygen species observed in XPS results, which favour removal of carbonaceous species through oxidation, generating carbon oxides. Impregnation catalysts present similar surface carbon content, which agrees with their observed similar performance in the process.

4. CONCLUSIONS

In this work, catalysts based in Mn and Ce were prepared by two methods, co-precipitation and impregnation, in order to study the effect of physicochemical properties and catalytic performance on the simultaneous reduction of NO and o-DCB oxidation. Characterization results showed that each preparation method favors different interaction between Mn and Ce. Thus, Mn is loaded on CeO_2 in impregnation catalysts, whereas Mn incorporates to the CeO_2 structure in co-precipitation catalysts, creating a solid solution. The formation of the solid solution plays an important role, because it enhances the redox properties through the generation of oxygen vacancies, which improve oxygen mobility. Moreover, an increase of acid properties is also provided by the high interaction between both metals.

The catalytic tests have corroborated the better activity of catalysts prepared by co-precipitation, with increased NO and o-DCB conversion at low temperature compared to impregnation catalysts. In this way, catalysts above 80 mol.% MnO_X showed the best catalytic activity, with NO conversions above 90% at temperatures below 250 ºC and o-DCB conversions above 80% at temperatures above 200 ºC. In these catalysts, XRD and TPR evidenced coexistence of Mn_2O_3 crystals and the solid solution, which could be responsible for the great catalytic performance. Regarding to selectivity, N_2O and NO_2 were the main by-products of SCR reaction in both impregnation and co-precipitation catalysts. N_2O is produced in all temperature range, whereas NO_2 is observed above 300 ºC. The formation of these compounds is favored by the improvement of oxidation properties, which are clearly related to Mn species. In oxidation reaction, co-precipitation catalysts present slightly higher

selectivity to CO_2, above 80%. However, an increase of selectivity to CO and chlorinated by-products production at medium temperature evidenced a possible change in the oxidation pathway, in which higher amount of oxidation intermediates is involved. Stability tests evidenced deactivation in all catalysts, mainly in the oxidation reaction. Deactivation is affected by preparation method and Mn content in co-precipitation catalysts and is associated to Cl adsorption, which is also detrimental for total oxidation of o-DCB.

5. ACKNOWLEDGMENTS

The authors thank MINECO/FEDER (CTQ2015-64616-P), The Basque Government (IT657-13 and IT1297-19) and the University of the Basque Country UPV/EHU (INF12/37, UFI 11/39) for the economic support. The author JAMM specially acknowledges MINECO/FEDER (BES-2016-077849) for the PhD grant. Likewise, the authors thank technical and human support provided by SGIker of UPV/EHU and European funding (ERDF and ESF).

REFERENCES

[1] M. Goemans, P. Clarysse, J. Joannès, P. De Clercq, S. Lenaerts, K. Matthys, K. Boels, Catalytic NO_X reduction with simultaneous dioxin and furan oxidation,50 (2003) 489-497.
https://doi.org/10.1016/S0045-6535(02)00554-4.

[2] E. Finocchio, G. Busca, M. Notaro, A review of catalytic processes for the destruction of PCDD and PCDF from waste gases, Appl. Catal. B Environ. 62 (2006) 12-20.
https://doi.org/10.1016/j.apcatb.2005.06.010.

[3] G. Qi, R.T. Yang, Low-temperature selective catalytic reduction of NO with NH_3 over iron and manganese oxides supported on titania, Appl. Catal. B Environ. 44 (2003) 217-225.
https://doi.org/10.1016/S0926-3373(03)00100-0.

[4] F. Gao, X. Tang, H. Yi, S. Zhao, C. Li, J. Li, Y. Shi, X. Meng, A review on selective catalytic reduction of NO_X by NH_3 over Mn–based catalysts at low temperatures: Catalysts, mechanisms, kinetics and DFT calculations, Catalysts 7 (2017).
https://doi.org/10.3390/catal7070199.

[5] M. Gallastegi-Villa, A. Aranzabal, Z. Boukha, J.A. González-Marcos, J.R. González-Velasco, M.V. Martínez-Huerta, M.A. Bañares, Role of surface vanadium oxide coverage support on titania for the simultaneous removal of o-dichlorobenzene and NO_x from waste incinerator flue gas, Catal Today. 254 (2015) 2-11.
https://doi.org/10.1016/j.cattod.2015.02.029.

[6] S. Zhang, B. Zhang, B. Liu, S. Sun, A review of Mn-containing oxide catalysts for low temperature selective catalytic reduction of NO_X with NH_3: Reaction mechanism and catalyst deactivation, RSC Adv. 7 (2017) 26226-26242.
https://doi.org/10.1039/c7ra03387g.

[7] R. Jin, Y. Liu, Z. Wu, H. Wang, T. Gu, Low-temperature selective catalytic reduction of NO with NH_3 over Mn-Ce oxides supported on TiO_2 and Al_2O_3 : A comparative study, Chemosphere 78 (2010) 1160-1166.
https://doi.org/10.1016/j.chemosphere.2009.11.049.

[8] K. Qi, J. Xie, Z. Zhang, D. Fang, D. Han, X. Liu, P. Gong, F. Li, F. He, Facile large-scale synthesis of Ce–Mn composites by redox-precipitation and its superior low-temperature performance for NO removal, Powder Technol. 338 (2018) 774-782.
https://doi.org/10.1016/j.powtec.2018.07.073.

[9] B. Thirupathi, P.G. Smirniotis, Co-doping a metal (Cr, Fe, Co, Ni, Cu, Zn, Ce, and Zr) on Mn/TiO_2 catalyst and its effect on the selective reduction of NO with NH_3 at low-temperatures, Appl. Catal. B Environ. 110 (2011) 195-206.

https://doi.org/10.1016/j.apcatb.2011.09.001.

[10] X. Wang, L. Zhang, S. Wu, W. Zou, S. Yu, Y. Shao, L. Dong, Promotional effect of Ce on iron-based catalysts for selective catalytic reduction of NO with NH_3, Catalysts 6 (2016).
https://doi.org/10.3390/catal6080112.

[11] Y. Wan, W. Zhao, Y. Tang, L. Li, H. Wang, Y. Cui, J. Gu, Y. Li, J. Shi, Ni-Mn bi-metal oxide catalysts for the low temperature SCR removal of NO with NH_3, Appl. Catal. B Environ. 148-149 (2014) 114-122.
https://doi.org/10.1016/j.apcatb.2013.10.049.

[12] M. Kang, T.H. Yeon, E.D. Park, J.E. Yie, J.M. Kim, Novel MnO_X catalysts for NO reduction at low temperature with ammonia, Catal Lett. 106 (2006) 77-80.
https://doi.org/10.1007/s10562-005-9194-3.

[13] J. Li, J. Chen, R. Ke, C. Luo, J. Hao, Effects of precursors on the surface Mn species and the activities for NO reduction over MnO_X/TiO_2 catalysts, Catal. Commun. 8 (2007) 1896-1900.
https://doi.org/10.1016/j.catcom.2007.03.007.

[14] V.P. Santos, M.F.R. Pereira, J.J.M. Órfão, J.L. Figueiredo, The role of lattice oxygen on the activity of manganese oxides towards the oxidation of volatile organic compounds, Appl. Catal. B Environ. 99 (2010) 353-363.
https://doi.org/10.1016/j.apcatb.2010.07.007.

[15] Z. Liu, Y. Yi, S. Zhang, T. Zhu, J. Zhu, J. Wang, Selective catalytic reduction of NO_X with NH_3 over Mn-Ce mixed oxide catalyst at low temperatures, Catal Today. 216 (2013) 76-81.
https://doi.org/10.1016/j.cattod.2013.06.009.

[16] G. Qi, R.T. Yang, R. Chang, MnO_X-CeO_2 mixed oxides prepared by co-precipitation for selective catalytic reduction of NO with NH_3 at low temperatures, Appl. Catal. B Environ. 51 (2004) 93-106.
https://doi.org/10.1016/j.apcatb.2004.01.023.

[17] B. Shen, X. Zhang, H. Ma, Y. Yao, T. Liu, A comparative study of Mn/CeO_2, Mn/ZrO_2 and Mn/Ce-ZrO_2 for low temperature selective catalytic reduction of NO with NH_3 in the presence of SO_2 and H_2O, J. Environ. Sci. 25 (2013) 791-800.
https://doi.org/10.1016/S1001-0742(12)60109-0.

[18] X. Wang, L. Ran, Y. Dai, Y. Lu, Q. Dai, Removal of Cl adsorbed on Mn-Ce-La solid solution catalysts during CVOC combustion, J. Colloid Interface Sci. 426 (2014) 324-332.
https://doi.org/10.1016/j.jcis.2013.10.007.

[19] W. Xingyi, K. Qian, L. Dao, Catalytic combustion of chlorobenzene over MnO_X-CeO_2 mixed oxide catalysts, Appl. Catal. B Environ. 86 (2009) 166-175.

https://doi.org/10.1016/j.apcatb.2008.08.009.

[20] Y. Wu, Y. Zhang, M. Liu, Z. Ma, Complete catalytic oxidation of o-xylene over Mn-Ce oxides prepared using a redox-precipitation method, Catal Today. 153 (2010) 170-175.
https://doi.org/10.1016/j.cattod.2010.01.064.

[21] X. Yao, K. Ma, W. Zou, S. He, J. An, F. Yang, L. Dong, Influence of preparation methods on the physicochemical properties and catalytic performance of MnO_X-CeO_2 catalysts for NH_3-SCR at low temperature, Cuihua Xuebao Chin. J. Catalysis. 38 (2017) 146-159.
https://doi.org/10.1016/S1872-2067(16)62572-X.

[22] B. Shen, F. Wang, T. Liu, Homogeneous MnO_X-CeO_2 pellets prepared by a one-step hydrolysis process for low-temperature NH_3-SCR, Powder Technol. 253 (2014) 152-157.
https://doi.org/10.1016/j.powtec.2013.11.015.

[23] G. Picasso, M. Gutiérrez, M.P. Pina, J. Herguido, Preparation and characterization of Ce-Zr and Ce-Mn based oxides for n-hexane combustion: Application to catalytic membrane reactors, Chem. Eng. J. 126 (2007) 119-130.
https://doi.org/10.1016/j.cej.2006.09.005.

[24] Q. Shen, L. Zhang, N. Sun, H. Wang, L. Zhong, C. He, W. Wei, Y. Sun, Hollow MnO_X-CeO_2 mixed oxides as highly efficient catalysts in NO oxidation, Chem. Eng. J. 322 (2017) 46-55.
https://doi.org/10.1016/j.cej.2017.02.148.

[25] S. Ramana, B.G. Rao, P. Venkataswamy, A. Rangaswamy, B.M. Reddy, Nanostructured Mn-doped ceria solid solutions for efficient oxidation of vanillyl alcohol, J. Mol. Catal. A Chem. 415 (2016) 113-121.
https://doi.org/10.1016/j.molcata.2016.01.028.

[26] X. Wu, Q. Liang, D. Weng, J. Fan, R. Ran, Synthesis of CeO_2-MnO_X mixed oxides and catalytic performance under oxygen-rich condition, Catal Today. 126 (2007) 430-435.
https://doi.org/10.1016/j.cattod.2007.06.014.

[27] X. Wu, F. Lin, H. Xu, D. Weng, Effects of adsorbed and gaseous NO_X species on catalytic oxidation of diesel soot with MnO_X-CeO_2 mixed oxides, Appl. Catal. B Environ. 96 (2010) 101-109.
https://doi.org/10.1016/j.apcatb.2010.02.006.

[28] X. Tang, Y. Li, X. Huang, Y. Xu, H. Zhu, J. Wang, W. Shen, MnO_X-CeO_2 mixed oxide catalysts for complete oxidation of formaldehyde: Effect of preparation method and calcination temperature, Appl. Catal. B Environ. 62 (2006) 265-273.
https://doi.org/10.1016/j.apcatb.2005.08.004.

[29] F. Bertinchamps, C. Grégoire, E.M. Gaigneaux, Systematic investigation of supported transition metal oxide based formulations for the catalytic oxidative elimination of (chloro)-aromatics. Part I: Identification of the optimal main active phases and supports, Appl. Catal. B Environ. 66 (2006) 1-9. https://doi.org/10.1016/j.apcatb.2006.02.011.

[30] M.A. Larrubia, G. Busca, An FT-IR study of the conversion of 2-chloropropane, o-dichlorobenzene and dibenzofuran on V_2O_5 -MoO_3-TiO_2 SCR-deNO_X catalysts, Appl. Catal. B Environ. 39 (2002) 343-352. https://doi.org/10.1016/S0926-3373(02)00116-9.

[31] S. Albonetti, S. Blasioli, R. Bonelli, J.E. Mengou, S. Scirè, F. Trifirò, The role of acidity in the decomposition of 1,2-dichlorobenzene over TiO_2-based V_2O_5/WO_3 catalysts, Appl Catal A Gen. 341 (2008) 18-25. https://doi.org/10.1016/j.apcata.2007.12.033.

[32] H. Li, G. Lu, Q. Dai, Y. Wang, Y. Guo, Y. Guo, Efficient low-temperature catalytic combustion of trichloroethylene over flower-like mesoporous Mn-doped CeO_2 microspheres, Appl. Catal. B Environ. 102 (2011) 475-483. https://doi.org/10.1016/j.apcatb.2010.12.029.

[33] Q. Ye, B.-. Xu, Textural and structure characterizations of $Ce_{1-X}Mn_XO_2$ prepared by citric acid sol-gel method, Acta Phys. Chim. Sin. 22 (2006) 345-349. https://doi.org/10.3866/PKU.WHXB20060318.

[34] X. Du, D. Zhang, L. Shi, R. Gao, J. Zhang, Morphology dependence of catalytic properties of Ni/CeO_2 nanostructures for carbon dioxide reforming of methane, J. Phys. Chem. C. 116 (2012) 10009-10016. https://doi.org/10.1021/jp300543r.

[35] C. Tang, J. Li, X. Yao, J. Sun, Y. Cao, L. Zhang, F. Gao, Y. Deng, L. Dong, Mesoporous NiO-CeO_2 catalysts for CO oxidation: Nickel content effect and mechanism aspect, Appl Catal A Gen. 494 (2015) 77-86. https://doi.org/10.1016/j.apcata.2015.01.037.

[36] P. Venkataswamy, D. Jampaiah, C.U. Aniz, B.M. Reddy, Investigation of physicochemical properties and catalytic activity of nanostructured $Ce_{0.7}M_{0.3}O_2$ (M = Mn, Fe, Co) solid solutions for CO oxidation, J. Chem. Sci. 127 (2015) 1347-1360. https://doi.org/10.1007/s12039-015-0897-8.

[37] X. You, Z. Sheng, D. Yu, L. Yang, X. Xiao, S. Wang, Influence of Mn/Ce ratio on the physicochemical properties and catalytic performance of graphene supported MnO_X-CeO_2 oxides for NH_3-SCR at low temperature, Appl. Surf. Sci. 423 (2017) 845-854. https://doi.org/10.1016/j.apsusc.2017.06.226.

[38] C.M. Julien, M. Massot, C. Poinsignon, Lattice vibrations of manganese oxides: Part I. Periodic structures, Spectrochim. Acta Part A Mol. Biomol. Spectrosc. 60 (2004) 689-700. https://doi.org/10.1016/S1386-1425(03)00279-8.

[39] H. Chen, A. Sayari, A. Adnot, F. Larachi, Composition-activity effects of Mn-Ce-O composites on phenol catalytic wet oxidation, Appl. Catal. B Environ. 32 (2001) 195-204. https://doi.org/10.1016/S0926-3373(01)00136-9.

[40] X. Tang, J. Li, L. Sun, J. Hao, Origination of N_2O from NO reduction by NH_3 over β-MnO_2 and α-Mn_2O_3, Appl. Catal. B Environ. 99 (2010) 156-162. https://doi.org/https://doi.org/10.1016/j.apcatb.2010.06.012.

[41] E.R. Stobbe, B.A. De Boer, J.W. Geus, The reduction and oxidation behaviour of manganese oxides, Catal Today. 47 (1999) 161-167. https://doi.org/10.1016/S0920-5861(98)00296-X.

[42] Z. Wu, N. Tang, L. Xiao, Y. Liu, H. Wang, MnO_X/TiO_2 composite nanoxides synthesized by deposition-precipitation method as a superior catalyst for NO oxidation, J. Colloid Interface Sci. 352 (2010) 143-148. https://doi.org/10.1016/j.jcis.2010.08.031.

[43] Y. Wang, X. Li, L. Zhan, C. Li, W. Qiao, L. Ling, Effect of SO_2 on activated carbon honeycomb supported CeO_2-MnO_X catalyst for NO removal at low temperature, Ind Eng Chem Res. 54 (2015) 2274-2278. https://doi.org/10.1021/ie504074h.

[44] M.D.H. Chowdhury, J.G. Um, J. Jang, Remarkable changes in interface O vacancy and metal-oxide bonds in amorphous indium-gallium-zinc-oxide thin-film transistors by long time annealing at 250 °C, Appl. Phys. Lett. 105 (2014). https://doi.org/10.1063/1.4903874.

[45] C. Bozo, N. Guilhaume, J. Herrmann, Role of the ceria-zirconia support in the reactivity of platinum and palladium catalysts for methane total oxidation under lean conditions, J. Catal. 203 (2001) 393-406. https://doi.org/10.1006/jcat.2001.3320.

[46] S. Ponce, M.A. Peña, J.L.G. Fierro, Surface properties and catalytic performance in methane combustion of SR-substituted lanthanum manganites, Appl. Catal. B Environ. 24 (2000) 193-205. https://doi.org/10.1016/S0926-3373(99)00111-3.

[47] J. Chen, M. Shen, X. Wang, G. Qi, J. Wang, W. Li, The influence of nonstoichiometry on $LaMnO_3$ perovskite for catalytic NO oxidation, Appl. Catal. B Environ. 134-135 (2013) 251-257. https://doi.org/10.1016/j.apcatb.2013.01.027.

[48] Y. Dai, X. Wang, Q. Dai, D. Li, Effect of Ce and La on the structure and activity of MnO_X catalyst in catalytic combustion of chlorobenzene, Appl. Catal. B Environ. 111-112 (2012) 141-149. https://doi.org/10.1016/j.apcatb.2011.09.028.

[49] S. Ren, J. Yang, T. Zhang, L. Jiang, H. Long, F. Guo, M. Kong, Role of cerium in improving NO reduction with NH_3 over Mn–Ce/ASC catalyst in low-temperature flue gas, Chem. Eng. Res. Des. 133 (2018) 1-10. https://doi.org/10.1016/j.cherd.2018.02.041.

[50] T.S. Park, S.K. Jeong, S.H. Hong, S.C. Hong, Selective catalytic reduction of nitrogen oxides with NH_3 over natural manganese ore at low temperature, Ind Eng Chem Res. 40 (2001) 4491-4495. https://doi.org/10.1021/ie010218.

[51] M. Kang, E.D. Park, J.M. Kim, J.E. Yie, Manganese oxide catalysts for NO_X reduction with NH_3 at low temperatures, Appl Catal A Gen. 327 (2007) 261-269. https://doi.org/10.1016/j.apcata.2007.05.024.

[52] C. Wang, F. Yu, M. Zhu, C. Tang, K. Zhang, D. Zhao, L. Dong, B. Dai, Highly selective catalytic reduction of NO_X by MnO_X–CeO_2–Al_2O_3 catalysts prepared by self-propagating high-temperature synthesis, J. Environ. Sci. 75 (2019) 124-135. https://doi.org/10.1016/j.jes.2018.03.011.

[53] J. Lichtenberger, M.D. Amiridis, Catalytic oxidation of chlorinated benzenes over V_2O_5/TiO_2 catalysts, J. Catal. 223 (2004) 296-308. https://doi.org/10.1016/j.jcat.2004.01.032.

[54] J. Kan, L. Deng, B. Li, Q. Huang, S. Zhu, S. Shen, Y. Chen, Performance of co-doped Mn-Ce catalysts supported on cordierite for low concentration chlorobenzene oxidation, Appl Catal A Gen. 530 (2017) 21-29. https://doi.org/10.1016/j.apcata.2016.11.013.

[55] C.E. Hetrick, F. Patcas, M.D. Amiridis, Effect of water on the oxidation of dichlorobenzene over V_2O_5/TiO_2 catalysts, Appl. Catal. B Environ. 101 (2011) 622-628. https://doi.org/10.1016/j.apcatb.2010.11.003.

TABLE AND FIGURE CAPTIONS

Table 1: Textural properties of the catalysts.

Table 2: Redox and acidic properties of the catalysts.

Table 3: XPS results of catalysts. Binding energies and surface atomic relations.

Table 4: Chlorine and carbon contents of used catalysts after stability tests.

Fig. 1: Experimental set-up.

Fig. 2: XRD patterns of A) co-precipitation catalysts and B) impregnation catalysts.

Fig. 3: Raman spectra of A) co-precipitation catalysts and B) impregnation catalysts.

Fig. 4: TPR profiles of A) co-precipitation catalysts and B) impregnation catalysts.

Fig. 5: XPS spectra of co-precipitation catalysts: A) Ce 3d 5/2 C) Mn 2p E) O 1s; and impregnation catalysts: B) Ce 3d 5/2 D) Mn 2p F) O 1s.

Fig. 6: NH_3-TPD profiles of A) Co-precipitation catalysts and B) impregnation catalysts.

Fig. 7: Catalytic activity of co-precipitation catalysts: A) NO conversion and C) o-DCB conversion; and impregnation catalysts B) NO conversion and D) o-DCB conversion. Gas composition: 100 ppm o-DCB, 300 ppm NO, 300 ppm NH_3 and 10% O_2 at 1.5 atm 2 L_N min^{-1} and 60 L_N $(h \cdot g)^{-1}$.

Fig. 8: N_2O concentration of A) co-precipitation catalysts C) impregnation catalysts; NO_2 concentration B) co-precipitation catalysts D) impregnation catalysts.

Fig. 9: CO_2 selectivity of A) co-precipitation catalysts C) impregnation catalysts; CO selectivity B) co-precipitation catalysts D) impregnation catalysts.

Fig. 10: Chlorinated by-products produced in o-DCB oxidation reaction by co-precipitation catalysts A) Tetrachloroethylene B) Trichlorobenzene; and impregnation catalysts C) Tetrachloroethylene D) Trichlorobenzene.

Fig. 11: Stability test of co-precipitation and impregnation Mn-contain catalysts at 300 ºC. Gas composition: 100 ppm o-DCB, 300 ppm NO, 300 ppm NH_3 and 10% O_2 at 1.5 atm, 2 L_N min^{-1} and 60 L_N $(h \cdot g)^{-1}$. A) NO conversions B) o-DCB conversions C) N_2O and NO_2 concentrations D) CO_2 and CO concentrations.

Effect of Preparation Procedure and Composition of Catalysts based on Mn and Ce Oxides in the Simultaneous Removal of NO_X and o-DCB

J.A. Martín-Martín, J. Sánchez-Robles, M.P. González-Marcos, A. Aranzabal, J.R. González-Velasco

Group of Chemical Technologies for Environmental Sustainability

Dept. of Chemical Engineering, Faculty of Science and Technology

The University of the Basque Country, UPV/EHU; P.O. Box 644, E-48080 Bilbao, Spain

mp.gonzalezmarcos@ehu.es

ABSTRACT

Two series of catalysts based on Mn and Ce oxides were prepared by co-precipitation and impregnation, in order to study their physicochemical properties and catalytic performance in the simultaneous reduction of NO and oxidation of o-DCB. Co-precipitation catalysts showed better activity than those prepared by impregnation because of the formation of a MnO_X-CeO_2 solid solution, which improves redox and acid properties. Moreover, the catalysts with MnO_X content between 80 and 90 mol.%, in which a coexistence between solid solution phase and Mn_2O_3 crystal was found, presented NO conversion above 90% at temperatures below 250 ºC and o-DCB conversion above 80% at temperatures above 200 ºC. The main by-products of SCR were N_2O, produced in the whole range of temperature, and NO_2, formed at temperatures above 300 ºC. Selectivity to CO_2 above 80% was obtained using co-precipitation catalysts in all temperature range. Deactivation experiments showed that oxidation reaction strongly contributes to deactivate impregnation catalysts, whereas the effect of deactivation is lower in co-precipitation catalysts at high Mn contents.

Keywords

MnO_X and CeO_2; Co-precipitation; Impregnation; o-DCB; NH_3-SCR.

1. INTRODUCTION

Simultaneous catalytic abatement of nitrogen oxides (NO_X) and polychlorinated dibenzo dioxins and furans (PCDD/Fs) is an alternative to the present techniques for elimination of both pollutants in municipal solid waste (MSW) incineration plants, in line with the continuous development of more efficient technologies due to the tightening of environment laws. In this process, both pollutants are removed in the same catalytic reactor [1,2]. The elimination of NO_X occurs through Selective Catalytic Reduction (SCR) with NH_3, while PCDD/Fs are removed by catalytic oxidation, according to:

$$4NO + 4NH_3 + O_2 \rightarrow 4N_2 + 6H_2O \quad (1)$$

$$C_{12}H_nCl_{8-n}O_2 + (9+0.5n)O_2 \rightarrow (n-4)H_2O + 12CO_2 + (8-n)HCl \quad (2)$$

This is a highly interesting process, since it combines the advantages of SCR, such as high efficiency and low cost, with those of catalytic oxidation, in which the pollutants are completely oxidized. This way, the use of other techniques, such as adsorption or absorption, which generate a waste that needs further treatment or disposal [2], is avoided.

Commercial catalysts for SCR are VO_X/TiO_2 promoted by WO_X or MoO_X [3,4]. The same catalysts are the main option for catalytic oxidation of PCDD/Fs and chlorinated benzenes [2], the latter commonly used as model compounds of PCDD/Fs for laboratory experiments, because they are safer to handle and have a similar structure. The fact that the same formulation is used for the removal of both types of pollutants is the key for this application in which NO_X and PCDD/Fs are removed simultaneously. Recently, Gallastegi-Villa et al. reported that the simultaneous abatement of NO and o-dichlorobenzene (o-DCB, model compound of PCDD/Fs) with VO_X/TiO_2 is possible [5]. However,

these catalysts are not efficient enough, because NO reduction occurs at lower temperatures than o-DCB oxidation, whereas NO conversion decreases at temperatures where o-DCB conversion is high [5].

Currently, SCR commercial systems are demanding to work at lower temperatures because they are located at the end of the cleaning gas line in order to avoid catalyst poisoning by SO_2 [6]. As a consequence, a reheat of the flue gas is needed up to the operating temperature of SCR reactor [7,8], which involves high costs. The development of alternative catalytic formulations is of great interest for decreasing operation temperature of SCR systems and obtaining oxidation of PCDD/Fs at lower temperatures.

In this sense, transition metals oxides (CuO_X, FeO_X, MnO_X, NiO_X, ZrO_X) as catalysts for low-temperature SCR have been widely researched [9-11]. MnO_X-based catalysts are specifically gaining much attention in recent years because of the high oxidation states and characteristic crystal structure [4]. Kang et al. reported NO conversions above 95% between 75 and 175 ºC with MnO_X supported over Al_2O_3 and CeO_2 [12], while Li et al. achieved total NO conversion between 150 and 200 ºC using TiO_2 as support [13]. The same way, their high efficiency in reduction/oxidation cycles and excellent oxygen migration ability are positive for the application of this type of catalysts in the oxidation of chlorinated organic compounds [14].

CeO_2 has been widely studied for its great redox properties and high oxygen mobility related to oxygen vacancies [3,7,15]. These are properties that benefit the faster oxidation of NO to NO_2 and chlorinated organic compound, involved in fast SCR and catalytic oxidation, respectively. Therefore, the addition of CeO_2 to MnO_X-based catalysts may improve the catalytic performance in the

simultaneous abatement of NO_X and PCDD/Fs. The enhancement of catalytic activity in NO reduction has been corroborated by several works. Qi et al. reported NO conversion of 95% at 150 ºC with MnO_X-CeO_2 mixed oxide catalysts [16]. Similar results where showed by Shen et al. in MnO_X/CeO_2 supported catalyst between 120 and 220 ºC [17]. The same way, the MnO_X-CeO_2 formulation leads to the catalytic oxidation of chlorobenzene above 250 ºC [18,19] and o-xylene above 220 ºC [20].

It has been reported that physicochemical properties and catalytic performance depend on preparation methods [21,22]. Regarding to literature, several routes have been used for the preparation of MnO_X-CeO_2 catalysts, such as co-precipitation [23-25], sol-gel [26,27], impregnation [17], modified co-precipitation [28] and redox precipitation [8,20]. Unfortunately, no agreement about what preparation method is the most suitable for the simultaneous abatement of NO_X and PCDD/Fs is found in the literature. This is due to the small number of works focused on the elimination of both pollutants simultaneously, rather than independently.

In this work, catalysts based on Mn and Ce oxides were prepared by two methods, characterized by different techniques and tested in the simultaneous abatement of NO and o-DCB, through NH_3-SCR and catalytic oxidation, respectively. The catalytic test was carried out in conditions close to those used in MSW incineration plants. Therefore, the goal of this work is to evaluate the influence of preparation method in physicochemical properties and catalytic performance of the catalysts, in order to conclude the optimum preparation method and composition.

2. EXPERIMENTAL

2.1. Catalysts preparation

Two series of catalysts based on Mn and Ce oxides were prepared to different metal contents by co-precipitation and impregnation, in order to obtain solids with different properties. The experimental procedure followed in each preparation method is explained in detail in the following.

2.1.1. Co-precipitation method

The necessary amount of a solution of $Mn(NO_3)_2 \cdot 4H_2O$ in distilled water (0.55 M Mn) and/or a solution of $Ce(NO_3)_3 \cdot 6H_2O$ in distilled water (0.35 M Ce) were mixed at room temperature under magnetic stirring and co-precipitated by dropwise addition of a 1.3 M solution of NH_2COONH_4 until the solution reached pH = 9. The resulting suspension was aged during 2 h, then filtered and washed with distilled water. The obtained solid was dried at 110 ºC for 12 h and calcined at 500 ºC for 3 h.

With this procedure, solids with a bulk homogeneous composition of the oxides are obtained, in which Mn and Ce can belong to a common oxide structure, and/or be segregated in structures characteristic of their typical oxides. In order to carry out the catalytic reactions in the absence of mass transfer limitations and with low pressure drop, the catalysts were pelletized, crushed and sieved to 0.3-0.5 mm.

Seven catalysts were prepared by this procedure, from pure CeO_2 to pure MnO_X, with five intermediate compositions, and named: 0Mn-100Ce (pure CeO_2), 15Mn-85Ce, 50Mn-50Ce, 80Mn-20Ce, 85Mn-15Ce, 90Mn-10Ce and 100Mn-0Ce (pure MnO_X); where the numbers indicate the molar percentage of each oxide in the samples.

2.1.2. Impregnation method

CeO_2 support was prepared by thermal decomposition of $Ce(NO_3)_3 \cdot 6H_2O$ at 550 ºC for 3 h. Then, an aqueous solution with the proper amount of $Mn(NO_3)_2 \cdot 4H_2O$ was used to impregnate this support. The precursor solution and the support (2 mL/g) were mixed in a rotary evaporator, where the resulting slurry was kept in contact in continuous stirring for 1 h to improve homogeneity. Then, the solvent was evaporated by increasing the temperature to 40 ºC in vacuum conditions. Finally, the solid was dried at 110 ºC for 12 h, calcined at 500 ºC for 3 h and pelletized, crushed and sieved to 0.3-0.5 mm.

With this procedure, supported catalysts are obtained, in which the active phase, MnO_X, is located on the surface of the CeO_2 support to different surface coverage. Six catalysts were prepared by this procedure, with Mn content ranging from 0 to 8 wt.%, and named: $0Mn/CeO_2$ (the support, pure CeO_2), $1Mn/CeO_2$, $2Mn/CeO_2$, $3Mn/CeO_2$, $5Mn/CeO_2$ and $8Mn/CeO_2$. In order to complete the series, an additional sample of pure manganese oxide (named as MnO_X) was prepared by thermal decomposition of $Mn(NO_3)_2 \cdot 4H_2O$ at 500 ºC for 3 h.

2.1.3. Comparison between preparation methods

Taking into account both preparation methods, global composition of both catalyst series is very different. However, comparison can be made in terms of surface coverage of MnO_X, taking into account that catalysis is a surface phenomenon. Both series of catalysts have been prepared with the idea to cover the whole range of surface coverages, from 0 (pure CeO_2) to 1 (pure MnO_X).

In co-precipitation catalysts, molar composition gives a direct estimation of theoretical relative surface coverage, and that is the reason why composition of these catalysts is given as molar percentage of the oxides all over the paper.

In impregnation catalysts, MnO_X is only located at the surface. Thus, Mn content remains much smaller for similar surface coverage. In these catalysts, compositions are usually given as weight percentage of the active metal, and that is the reason why composition of these catalysts is given as wt.% Mn all over the paper. Taking into account the cross sectional area of MnO_X [29], the specific surface area of the support (CeO_2) and the probable multilayer deposition at high coverage, the $8Mn/CeO_2$ sample should very nearly approach total MnO_X surface coverage.

2.2. Catalyst characterization

2.2.1. XRD analysis

X-ray diffraction (XRD) was conducted on a Philips PW 1710 X-ray diffractometer with Cu Kα radiation (λ = 1.5406 Å) and Ni filter. The finely ground samples were scanned between 10° and 100° (2θ) with a 2θ step size of 0.026°º and counting time of 528 s. Crystal phases were identified by comparison with JCPDS (Joint Committee on Powder Diffraction Standards) database cards.

2.2.2. Textural properties

Textural properties were evaluated by N_2 adsorption–desorption isotherms at −196 ºC, in a Micromeritics TRISTAR II 3020. Specific surface areas of the catalysts were calculated by the standard BET procedure, using adsorption branch data in the relative equilibrium pressure range of 0.03-0.3. Pore average

size and distribution were calculated using the BJH method from the desorption branch. The samples (15–20 mg) were previously degassed under nitrogen flow at 350 ºC for 4 h.

2.2.3. Raman spectroscopy

Raman spectroscopy was performed in a Renishaw System 1000 Raman spectrometer. A 514 nm solid-state laser was used as excitation line with a power on the sample of 1 mW. All measurements were carried out at room temperature.

2.2.4. H_2-TPR analysis

Temperature programmed reduction with H_2 (H_2-TPR) was used to evaluate the redox properties of the catalysts. The experiments were performed on a Micromeritics AutoChem 2920 instrument. First of all, the samples (15-20 mg) were pre-treated under 50 cm^3/min of 5% O_2/He mixture at 500 ºC for 45 min and cooled down to 40 ºC in helium. Then, the samples were heated from 40 to 950 ºC with a rate of 10 ºC/min under 50 cm^3/min of 5% H_2/Ar. The water produced by reduction was trapped in a cold trap, and the consumption of H_2 was continuously monitored with a TCD. Total H_2 consumption was calculated from time-integration of TCD signal.

2.2.5. XPS characterization

X-ray Photoelectron Spectroscopy (XPS) was performed on an Al Kα (1486.6 eV) SPECS system (Berlin, Germany) equipped with 1D-150 Phoibos DLD analyzer and monochromatic radiation source. Detailed analysis of the elements (energy step 0.1 eV, dwell time 0.1 s, pass energy 30 eV) was performed with an electron exit angle of 90°. The spectra were fitted by

CasaXPS 2.3.16 software, modeling the Gauss-Lorentzian contributions after background subtraction (Shirley).

2.2.6. NH_3-TPD analysis

Catalysts surface acidity was measured by temperature programmed desorption of ammonia (NH_3-TPD) carried out on a Micromeritics AutoChem 2920 instrument. Before adsorption, all samples (15-20 mg) were pretreated under 50 cm^3/min of 5% O_2/He mixture at 500 ºC for 45 min and cooled down to 40 ºC in helium. The adsorption step was performed by 130 cm^3/min of 1% NH_3/He mixture gas at 40 ºC during 60 min. Then, the samples were exposed to 130 cm^3/min of helium for 60 min in order to remove physisorbed NH_3 from the surface. TPD experiments started from 40 to 450 ºC with a heating rate of 10 ºC/min and helium as carrier. NH_3 desorbed from the catalysts was continuously monitored with a TCD. Total acidity was calculated by time-integration of TCD signal.

2.2.7. Elemental analysis

Elemental analyses of deactivated catalysts (after stability tests) were conducted by XRF and EDS, in the case of chlorine, and EDS for carbon. XRF analysis was conducted in a wavelength dispersive X-ray fluorescence sequential spectrometer (WDXRF, PANalytical, AXIOS model) with Rh tube. EDS analysis was performed in a Carl Zeiss EVO 40 equipped with an EDS detector (Oxford Instrument X-Max). The measurements were made at 20 kV of voltage, 100-400 pA of current and at 10 nm approximately.

2.3. Experimental reaction set-up and catalytic tests

The experimental reaction set-up is shown in Fig. 1. The gas mixture was prepared to simulate the actual MSW incinerator combustion gases. Due to the high toxicity and operational problems arising from working with PCDD/Fs, most researchers usually use model compounds, less toxic and with similar structure. Thus, in this work, o-DCB has been used as the alternative to PCDD/Fs [~~29~~30,~~30~~31]. The composition of catalytic reactor feed was: O_2 (10%), NO (300 ppm), NH_3 (300 ppm), o-DCB (100 ppm) and Ar to balance. Gas flows were regulated by gas mass flow controllers (Bronkhorst® High-Tech F-201CV), whereas o-DCB and water liquid stream was dosed by a Bronkhorst® High-Tech μ-Flow L01-AAA-99-0-20S mass flow controller. In order to avoid the complete evaporation of the liquid component and favor the homogenous mixture with the gas stream, a controlled-evaporator-mixed (Bronkhorst® High-Tech W-102A-111-K) was used. Moreover, all pipes were hot, avoiding gas adsorption and condensation. The catalytic bed was formed by 1.5 g of particulate catalyst (0.3–-0.5 mm) mixed with inert quartz (0.5–-0.8 mm) in order to fill a bed volume of 3 cm^3, resulting in a GHSV value of 40,000 h^{-1}. The fixed catalytic bed was inside a U-shaped tubular quartz reactor (13.6 mm internal diameter), which was heated into a convective-flow oven.

Fig. 1

An on-line gas chromatograph (Agilent Technologies 7890A) equipped with a HP-VOC capillary column and a 5975C mass selective detector was used to quantify o-DCB concentration in the reactor inlet and outlet streams and also to detect possible chlorinated byproduct compounds. Furthermore, NO, NO_2 and NH_3 were continuously measured by ultra-violet (ABB, Limas 21), whereas CO_2, CO and N_2O were analyzed by infrared (ABB, Uras 26). During reaction, NH_3 is

not measured due to the interference between o-DCB and the Limas 21 analyzer. Because of this, NH_3 was only measured before reaction, in order to verify its inlet concentration.

Before each experiment, the catalyst was pretreated with pure argon flow (2 L_N/min) at 200 ºC for 2 h in order to remove the compounds adsorbed on the surface. The catalytic activity was measured by light-off curves at a pressure of 1.5 atm by feeding a constant total flow of 2 L_N/min and increasing the temperature from 100 to 450 ºC with a constant heating rate of 1.5 ºC/min. Stability tests were carried out at 300 ºC, keeping this temperature constant during 24 hours.

NO and o-DCB conversions were calculated from Ec. (1) and (2), respectively, as:

$$X_{NO} = \frac{NO_{in} - NO_{out}}{NO_{in}} \cdot 100 \quad (3)$$

$$X_{oDCB} = \frac{oDCB_{in} - oDCB_{out}}{oDCB_{in}} \cdot 100 \quad (4)$$

and selectivity to CO_2 and CO with:

$$S_{CO_2} = \frac{CO_2}{6 \cdot (oDCB_{in} - oDCB_{out})} \cdot 100 \quad (5)$$

$$S_{CO} = \frac{CO}{6 \cdot (oDCB_{in} - oDCB_{out})} \cdot 100 \quad (6)$$

3. RESULTS

3.1. Catalysts characterization

3.1.1. XRD analysis

Fig. 2A and 2B shows the XRD patterns of the catalysts prepared by co-precipitation and impregnation, respectively. CeO_2 in co-precipitation and impregnation series, 0Mn-100Ce and 0Mn/CeO_2, show the same diffraction peaks of cerionite, characteristic of cubic fluorite structure (JCPDS, 00-004-0593). On the other hand, manganese oxide of co-precipitation and impregnation series, 100Mn-0Ce and MnO_X, present clearly different diffraction patterns. Diffraction peaks of 100Mn-0Ce are associated to α-Mn_2O_3 phase (JCPDS, 01-078-030), whereas those of MnO_X are related to both α-Mn_2O_3 and β-MnO_2 (JCPDS, 00-050-0866) phases.

In the co-precipitation series, peaks associated to fluorite structure show a shift to higher Bragg angles with increasing Mn content, which is associated to the contraction and distortion of the fluorite structure caused by Mn insertion forming a solid solution. Ionic radii of Mn^{4+} (0.53 Å), Mn^{3+} (0.65 Å) and Mn^{2+} (0.83 Å) are smaller than that of Ce^{4+} (1.01 Å), which produces the lattice parameter modification (decrease) with increasing Mn content shown in Table 1 [3132]. Additional evidence for the formation of a solid solution is the observed broadening of the diffraction peaks of fluorite phase, associated to the decrease of fluorite crystal size, with increasing Mn content (Table 1), which indicates a loss of crystallinity due to the structural defects caused by Mn insertion. Above 80 mol.% MnO_X, additional sharp diffraction peaks associated to Mn_2O_3 can be observed in Fig. 2A, caused by segregation from the fluorite structure because

of saturation [~~32~~33], in agreement with the increase in Mn_2O_3 crystal size with Mn content (Table 1).

In the impregnation series, only peaks associated to fluorite structure can be found up to 5 wt.% Mn. The absence of diffraction peaks associated to MnO_X indicates that Mn species are highly dispersed on the CeO_2 surface. However, a diffraction peak associated to MnO_2 appears at 37.6° in the 8Mn/CeO_2 sample, supported catalyst with the highest Mn content, which indicates that Mn tends to form crystal aggregates of MnO_2 over the support at high coverage. In this case, no insertion of Mn on CeO_2 lattice is observed, as lattice parameter in Table 1 remains constant with increasing Mn content.

Thus, co-precipitation catalysts above 80 mol.% MnO_X consist of a MnO_X-CeO_2 solid solution and Mn_2O_3 crystals, so that Mn in high oxidation states coexist in different phases at high Mn content. In impregnation catalysts, on the other hand, no solid solution is observed and Mn in the form of MnO_2 is only in contact with surface CeO_2.

Table 1

Fig. 2

3.1.2. Textural properties

BET surface area and pore volume of catalysts were measured by N_2 physisorption and the results are listed in Table 1. In general, surface area and pore volume of co-precipitation catalysts are higher than those of impregnation catalysts.

In the co-precipitation catalysts, surface area of the intermediate compositions is higher than that of the pure oxides (0Mn-100Ce and 100Mn-0Ce) and pore volume notably increases with Mn content. In impregnation catalysts, on the

other hand, increasing Mn content produces a decrease in surface area, and a maximum pore volume around 2Mn/CeO_2. The decrease in pore volume above 3 wt.% Mn is probably associated to the formation of larger particles of MnO_X blocking the CeO_2 porous structure.

These results indicate that interaction of MnO_X and CeO_2 in co-precipitation catalysts, observed in XRD, generates structural defects in the bulk leading to higher exposure of catalyst surface and pores compared to impregnation catalysts. This feature probably contributes to the enhancement of catalytic performance by the increase of reaction sites.

3.1.3. Raman spectroscopy

Raman spectroscopy is useful to obtain information about alterations into the structure of the catalysts through the investigation of metal-oxygen vibrations. Fig. 3A and 3B show Raman spectra of catalysts prepared by co-precipitation and impregnation, respectively.

Spectra of pure CeO_2 samples, 0Mn-100Ce and 0Mn/CeO_2, exhibit an intense band at 460 cm^{-1}, associated to F_{2g} vibration mode [~~33~~34,~~34~~35]. This band is related to symmetrical stretching vibration of the atoms belonging to the structure around Ce^{4+} [~~35~~36]; so, it will be affected by alteration in the environment of sublattice oxygen. The F_{2g} vibration mode is also detected in all catalysts containing both MnO_X and CeO_2.

In the co-precipitation series, increasing Mn content produces a shift of F_{2g} band to lower wavenumber, from 460 cm^{-1} in 0Mn-100Ce down to 446 cm^{-1} in 80Mn-20Ce catalyst. This result proves the modification of the CeO_2 structure by the incorporation of Mn, and corroborates the solid solution formation. Together with F_{2g} displacement, the increase of Mn content promotes the appearance of

a band at 597 cm^{-1}, associated to oxygen vacancies [~~35~~36]. Oxygen vacancies appear to compensate the negative charges generated by the incorporation of a doping cation with different nature and oxidation state [25]. Thus, the band at 597 cm^{-1} is another evidence of the formation of a solid solution in this series. Above 80 mol.% MnO_X, an additional band appears at 635 cm^{-1} overlapping with the band associated to oxygen vacancies. This band is associated to MnO_X and increases its intensity with Mn content, whereas F_{2g} gradually decreases, which confirms the change of lattice parameter observed by XRD [~~36~~37]. Pure MnO_X (100Mn-0Ce) shows bands at 693, 640 and 306 cm^{-1} associated to vibrational modes v_7, v_6~~,~~ and v_2 of α-Mn_2O_3 [~~37~~38] in agreement with the results of XRD.

In the impregnation series, the position of F_{2g} band does not change with increasing Mn content. Besides, no clear evidence of Mn-O stretching modes is observed in the spectra of the supported samples, not even in 8Mn/CeO_2, which denotes the good dispersion of Mn on the support surface in this series. Concerning pure MnO_X, bands at 760, 662, 553 and 317 cm^{-1} associated to vibrational modes v_8, v_6, v_5 and v_2 of β-MnO_2 can be observed, in accordance with the results of XRD.

Fig. 3

3.1.4. H_2-TPR analysis

Redox properties were investigated by H_2-TPR. Fig. 4A and 4B show the H_2 consumption curves of catalysts prepared by co-precipitation and impregnation, respectively. TPR profiles of CeO_2 in both series, 0Mn-100Ce and 0Mn/CeO_2 samples, are very similar. They show two broad peaks located around 430 and 830 ºC, related to surface and bulk CeO_2 reduction, respectively [15]. Redox

properties are enhanced to different extent by the presence of Mn in the catalysts with respect to those of CeO_2. This enhancement can be associated to structural defects generated by surface interaction in impregnation catalysts.

In the co-precipitation series, a reduction peak around 100 ºC can be observed in the catalysts up to 50 mol.% MnO_X, associated to surface isolated Mn ions "embedded" into CeO_2 lattice [19,~~38~~39]. Increasing Mn content, two strongly overlapped peaks at 266 and 300 ºC and an additional peak at 400 ºC appear. Pure manganese oxide, 100Mn-0Ce, presents two reduction peaks at 293 and 435 ºC, which fit very well with pure Mn_2O_3 reduction profile in the literature [~~39~~40,~~40~~41], in accordance with XRD results, as time-integration of the TPR profile reveals that H_2 consumed in the first peak is half that in the second, which agrees with the stoichiometry of two reduction steps: the first peak related to the reduction of Mn_2O_3 to Mn_3O_4 and the second to the reduction of Mn_3O_4 to MnO.

In the impregnation series, two clear reduction peaks around 320 and 410 ºC associated to MnO_X reduction can be observed. In addition, surface CeO_2 reduction is also present in the range 200-400 ºC, although it is difficult to distinguish. Pure manganese oxide sample, MnO_X, also shows two reduction peaks, but shifted to higher temperatures and strongly overlapped (compared to 100Mn-0Ce), at 406 and 532 ºC. Similar TPR profile is reported by Shen et al., who associated the first reduction peak to the reduction or MnO_2 and Mn_2O_3 to Mn_3O_4 and the second to the reduction of Mn_3O_4 to MnO [24].

Several works in the literature agree that MnO_2 reduction in catalysts is practically indistinguishable from that of Mn_2O_3. Thus, many authors associate H_2 consumption at low temperature (around 300 ºC) to the reduction of

MnO_2/Mn_2O_3 to Mn_3O_4, and H_2 consumption at intermediate temperature (around 400 ºC) to the reduction of Mn_3O_4 to MnO and surface CeO_2 [24,~~31~~32,~~41~~42], when explaining TPR profiles. However, the appearance of two overlapped peaks at low temperature in co-precipitation catalysts brings to light the reduction of different phases in high oxidation state: the reduction of Mn ions embedded into cerium oxide lattice and the reduction of MnO_X crystals well-dispersed over the catalysts. The high interaction between both phases is responsible for the strong overlapping or these two peaks in the TPR profile. It should be noted that the first reduction peak, located at 266 ºC, increases with Mn content. The same way, XRD results above showed that high Mn content favored the presence of bigger Mn_2O_3 crystals in the catalysts. As a result, we propose that the first reduction peak is associated to reduction of MnO_X crystals, which would have better accessibility to H_2 because they are segregated from the solid solution. On the other hand, the peak around 300 ºC is related to reduction of Mn incorporated to the CeO_2 structure. Therefore, the results obtained in TPR are in accordance with those obtained through other techniques, supporting the formation of the solid solution in the co-precipitation series.

In these catalysts, several species are observed depending on Mn content. Low Mn contents favor the presence of isolated Mn located into the CeO_2 structure, whereas high Mn content promotes its segregation from the solid solution, creating crystalline aggregates.

H_2 consumption in TPR has been summarized in Table 2. In the co-precipitation series, H_2 consumption increases with Mn content. In the impregnation series, this is also truth in general, but H_2 consumption of the support ($0Mn/CeO_2$) is

somewhat higher than that of the lowest Mn content sample (1Mn/CeO_2). The results of H_2 consumption have been used to estimate average oxidation state of Mn in the catalysts, assuming MnO as the final reduction state of Mn (and similar reduction of CeO_2), and these results have been also added to Table 2, together with the proportion of Mn^{3+} and Mn^{4+}.

In the co-precipitation series, increasing Mn content produces a decrease in average oxidation state of Mn in the catalyst. Thus, at low Mn content, 15Mn-85Ce sample, the calculated average Mn oxidation state is 4. For this catalyst, the results of characterization above showed that all Mn was incorporated to CeO_2 structure; consequently, Mn^{4+} is the main species promoted when Mn is inside CeO_2 structure. At high Mn content, above 80 mol.% MnO_X, average Mn oxidation state decreases to 3.2-3.3, which suggests a coexistence of Mn^{4+} and Mn^{3+} species. The appearance of Mn^{3+} is favoured by the formation of Mn_2O_3 crystals. Pure manganese oxide, 100Mn-0Ce sample, in fact, shows an average Mn oxidation state around 3 in good agreement with XRD results, where only peaks associated to Mn_2O_3 were observed.

In the impregnation series, error in the estimation can be important below 3 wt.% Mn. However, average Mn oxidation state is above 3.5 in 5Mn/CeO_2 and 8Mn/CeO_2 samples. This fact suggests that higher Mn coverage leads to agglomeration in bigger crystals (as concluded by XRD) in which Mn^{4+}, in the form of MnO_2, is the main oxidation state. MnO_X sample in this series shows an average Mn oxidation state around 3.1, in line with the mixture of Mn_2O_3 and MnO_2 observed in XRD.

Table 2

Fig. 4

3.1.5. XPS characterization

Surface composition and surface oxidation states of the elements in the catalysts were studied by XPS. Fig. 5 shows Ce 3d, Mn 2p and O 1s spectra of co-precipitation (Fig. 5A, 5C and 5E) and impregnation (Fig. 5B, 5D and 5F) catalysts. All binding energies are referenced to elemental carbon (C 1s) spectrum at 284.5 eV.

Ce 3d spectra (Fig. 5A and 5B) have only been analyzed by their 5/2 spin orbit doublet, because of the overlapping of Ce and Auger Mn line at high Mn content. Ce 3d 5/2 is deconvolved in 5 peaks with V notation for the assignment to Ce^{3+} and Ce^{4+}. Thus, V, V^{II} and V^{III} peaks are associated to Ce^{4+}, and V^{0} and V^{I} peaks to Ce^{3+} [~~42~~43,~~43~~44]. A clear presence of surface Ce^{4+} and Ce^{3+} is observed in all samples. In this way, surface ~~average Ce oxidation state~~proportion of both species in the catalysts was calculated by XPS integration, and the values are summarized in Table 3. Similar values are observed for both co-precipitation and impregnation catalysts, although with slightly higher proportion of Ce^{3+} surface species~~cerium is slightly more oxidized~~ in the impregnation series. Ce^{3+} species are commonly associated to surface oxygen vacancies [~~33~~34,~~44~~45].

Mn 2p spectra of the catalysts (Fig. 5C and 5D) show a spin-orbit doublet Mn 2p 3/2 and Mn 2p 1/2, which were deconvolved in three components related to Mn^{3+}, Mn^{4+} and a satellite [~~45~~46,~~46~~47], located around 641.0, 642.5 and 646.7 eV, respectively. The satellite peak intensity was weak in all samples compared to Mn^{3+} and Mn^{4+}. The presence of Mn^{3+} and Mn^{4+} is in accordance with the results obtained by XRD and TPR, in which both types of Mn species were detected. Surface proportion of both~~average~~ Mn species~~oxidation state of~~

~~all~~ in the samples was calculated by XPS integration, and the values are also summarized in Table 3.

In co-precipitation catalysts, all samples show similar oxidation state of Mn in the surface, around 3.5, which suggests that proportion of surface ~~average~~ Mn^{3+} and Mn^{4+} ~~oxidation state~~ is similar in all samples, and different from that in the bulk ~~average Mn oxidation state~~ (obtained by TPR, Table 2.). Apparently, surface and bulk proportion of Mn^{3+} and ~~average~~ Mn^{4+} ~~oxidation state~~ would be similar ~~for~~ in 50Mn-50Ce sample, the surface would be enriched in Mn^{3+} ~~would be more oxidized in the bulk that the surface~~ below 50 mol.% MnO_X, and the surface would be enriched in Mn^{4+} ~~more oxidized in the surface than the bulk~~ above 50 mol.% MnO_X.

On the other hand, surface proportion of ~~average~~ Mn^{3+} and Mn^{4+} ~~oxidation state~~ in impregnation catalysts is also the same in all samples, and similar to that of the co-precipitation series, the proportion of Mn^{3+} being higher ~~less oxidized~~ in the surface than ~~in~~ the bulk, in general.

The differences ~~found regarding to average~~between surface and bulk proportions ~~oxidation state~~ of Mn^{3+} and Mn^{4+} ~~depending on~~with preparation method at high Mn content are probably related to different MnO_X crystals promoted by each preparation method.

Fig. 5E and 5F show the O 1s spectra of catalyst samples. In the impregnation series, the high Ce content produces a decrease in conductivity of the samples, which causes unsuitable spectra for deconvolution. For this reason, only O 1s of co-precipitated catalysts was deconvolved in three peaks. Each peak is associated to different surface oxygen species.

In the co-precipitation series, pure CeO_2, 0Mn-100Ce sample, the peak at 529.5 eV (O^I) is associated to lattice oxygen. This peak is shifted to lower binding energy in Mn-containing catalysts, due to the formation of the solid solution. Although O 1s profile was not deconvolved in impregnation catalysts, a clear shift to lower binding energies is also observed in the peak located around 529.8 eV in the Mn-containing catalysts with respect to $0Mn/CeO_2$, as a consequence of the interaction between Mn and the support.

The intermediate binding energy peak, located around 531.2 eV (O^{II}), is related to adsorbed oxygen on the surface, whereas the high binding energy peak, at 533.2 eV (O^{III}), is associated to molecular water and carbonate species adsorbed on the catalysts [24,~~47~~48]. Yao et al. proposed a process of oxygen storage/release in which adsorbed oxygen is involved in the reduction of CeO_2 to Ce_2O_3 to form oxygen vacancies [21]. In this way, relative O^{II} concentration may give an approximation of the amount of oxygen vacancies present in the surface of the catalysts. Thus, $O^{II}/(O^I + O^{II} + O^{III})$ ratio has been calculated for the co-precipitation catalysts and summarized in Table 3. We can see that increasing Mn content promotes higher relative O^{II} concentration, which evidences an increase of the amount of oxygen active species involved in the formation of oxygen vacancies, useful for the activation of reactants of SCR and oxidation reactions.

Table 3

Fig. 5

3.1.6. NH_3-TPD analysis

Acid properties were studied by NH_3-TPD experiments. NH_3 desorption profiles of the catalysts prepared by co-precipitation and impregnation are shown in Fig.

6A and 6B, respectively. Acid properties are involved in the adsorption and activation of the compounds used in both SCR and oxidation reactions. The position of the NH_3 desorption peaks is associated to the strength of the acid sites. Thus, peaks located at low temperature will be related to NH_3 desorbed from weak acid sites, while the peaks located at high temperature are attributed to NH_3 desorption from strong acid sites [21,~~48~~49]. The amount of the acid sites is related to the integrated area of the peaks.

NH_3 desorption profiles of pure CeO_2 in both series, 0Mn-100Ce and 0Mn/CeO_2, show a peak around 110 ºC, associated to weak acidity, and a shoulder at 220 ºC, related to strong acidity.

In the co-precipitation series, low Mn content promotes strong acidity with respect to 0Mn-100Ce (an increase of the intensity of the peak at 220 ºC). Moreover, an increase of NH_3 desorption at temperatures around 160 ºC, broadening the low-temperature desorption peak, is observed above 80 mol.% MnO_X. This fact evidences that high Mn content produces an increase of weak acidity, probably associated to the Mn_2O_3 phase. Pure manganese oxide, 100Mn-0Ce sample, presents two desorption peaks at 100 and 187 ºC. Compared to the mixed oxides, peaks in 100Mn-0Ce are shifted to lower temperature, which indicates that the presence of Ce promotes stronger interaction between NH_3 and the catalysts and, thus, stronger acid sites, which may be caused by the enhancement of redox properties observed by TPR.

In the impregnation series, the presence of Mn contributes to increase the strong acidity because of the appearance of a peak at 220 ºC. No clear desorption peaks were observed for MnO_X sample, probably because of the low surface area of that sample (see Table 1).

Quantitative results for acidity, calculated by time-integration of the TCD signal, are summarized in Table 2. Comparison between the two catalyst series reveals that co-precipitation catalysts show higher acidity than impregnation catalysts, which may be associated to the higher interaction between Mn and Ce through the solid solution, taking into account that acidity is also higher per unit surface area (see Table 2). Moreover, different correlation between weak and strong acidity has been found depending on preparation method and composition.

In the impregnation series, higher Mn content promotes strong acidity in detriment of weak acidity. However, above 5 wt.% Mn (composition from which MnO_X crystals were detected by XRD) a decrease of both types of acidity is observed. Although this effect could partially be associated to lower surface area (see Table 1), the calculated acidity per unit area in Table 2 remains lower. Therefore, these results suggest that highly-disperse Mn is the species promoting catalyst acidity, and MnO_2 is detrimental for both weak and strong acidity.

Fig. 6

3.2. Catalytic performance

3.2.1. Catalytic activity

Fig. 7 shows simultaneous NO SCR and o-DCB oxidation catalytic activity of co-precipitation (Fig. 7A and 7B) and impregnation (Fig. 7C and 7D) catalysts. Co-precipitation catalysts are clearly more active than impregnation catalysts.

Concerning NO SCR, pure CeO_2 samples, 0Mn-100Ce and 0Mn/CeO_2, are active in SCR from 250 ºC, reaching the maximum NO conversion of 85% at 350 ºC, approximately.

The incorporation of Mn in co-precipitation catalysts (Fig. 7A) improves catalytic activity in SCR. At low Mn content (15Mn-85Ce catalyst) NO conversion profile is similar to that obtained with impregnation catalysts (Fig. 7C), although it does not enhance the one obtained with 100Mn-0Ce. Mn content above 50 mol.% MnO_X leads to NO conversion above 95% in the 100-200 ºC temperature range. NO conversion decays in the high-temperature range because of the appearance of side reactions (NH_3 oxidation), which consume the reactants involved in SCR.

In the impregnation catalysts (Fig. 7C), incorporation of Mn promotes an increase of NO conversion up to 70% at temperatures above 150 ºC. However, the further increase of temperature produces a decay of NO conversion, which increases again from 50 to 75% in the medium temperature range. Temperatures above 350 ºC produce a drastic drop of NO conversion in all catalysts. No great differences of NO conversion profiles have been observed among catalysts with MnO_X and CeO_2 in their composition, although the catalyst with the lowest Mn content favors slightly higher NO conversion at low temperature.

Comparing between both series, the temperature at which NO conversion starts to decrease is higher in impregnation catalysts and pure CeO_2 samples than in co-precipitation catalysts. This result suggests that Mn improves the oxidation properties of the catalysts, shifting NH_3 oxidation to lower temperatures.

Fig. 7

Regarding oxidation reaction, Fig. 7B and 7D, addition of MnO_X to CeO_2 promotes catalytic activity in both series of catalysts. o-DCB conversion profiles are similar in all catalysts: they show a maximum at low temperatures from which o-DCB conversion decays, and then strongly increases with temperature. o-DCB conversion values at low and high temperature depend on Mn content and preparation method.

In the co-precipitation series, 15Mn-85Ce sample showed similar results than impregnation catalysts (Fig. 7D), although with higher o-DCB conversion values (85 and 99% at 280 and 450 ºC, respectively). The increase of Mn content shifts o-DCB conversion profiles to lower temperatures. Thus, catalysts above 80 mol.% MnO_X present the best activity, with o-DCB conversions above 85% at 200 ºC, and total conversion at temperatures above 325ºC.

In the impregnation series, higher Mn loading increases catalytic activity, $5Mn/CeO_2$ and $8Mn/CeO_2$ being the best impregnation catalysts, with o-DCB conversion of 60 and 90% at 280 and 450 ºC, respectively. The similar decay of o-DCB conversion at medium temperature in both co-precipitation and impregnation catalysts should be noted, which could be attributed to oxidation occurring through different pathways depending on temperature.

Summarizing, catalysts with both MnO_X and CeO_2 in their composition, especially those with high Mn content, showed better catalytic performance than pure oxides in the simultaneous removal of NO and o-DCB. These results reveal that, although Mn species are the main contribution to catalytic activity, a little amount of Ce becomes important to reach higher conversion of o-DCB and total conversion of NO at low temperature. Moreover, catalysts prepared by co-precipitation showed the best catalytic activity, with higher NO and o-DCB

conversion at lower temperatures than impregnation catalysts. According to characterization, higher interaction between Mn and Ce was evidenced in co-precipitation catalysts, which bring to the light the relevance of the interaction between both metals as the key factor to improve catalytic activity in NO reduction and o-DCB oxidation.

Regarding to catalytic composition, co-precipitation catalysts above 80 mol.% MnO_X were found to present the best catalytic activity, leading to conversions above 80% of both NO and o-DCB in the temperature range of 180-300 ºC. In these catalysts, XRD results showed that they were not only composed by the solid solution of the oxides, but also by segregated Mn_2O_3 crystal aggregates. Moreover, TPR results showed that Mn tends to be as Mn^{4+} when inside CeO_2 structure, while as Mn^{3+} in Mn_2O_3 crystal aggregates. As a consequence, the synergy of both crystal phases provides Mn in different oxidation states, which is responsible for the great catalytic performances of high Mn content co-precipitation catalysts. This conclusion is in accordance with Dai et al., who proposed that Mn species in the interface between MnO_X and the solid solution and their neighbor lattice oxygen are the best active sites [~~47~~48].

3.2.2. Analysis of by-products

In SCR, N_2O and NO_2 were found to be the main by-products. The production profiles of both compounds are shown in Fig. 8 for co-precipitation (Fig. 8A and 8B) and impregnation (Fig. 8C and 8D) catalysts, respectively. In pure CeO_2 samples of both series, 0Mn-100Ce and 0Mn/CeO_2, N_2O production is below 30 ppm in all temperature range. However, the addition of Mn, even in samples with the lowest Mn content, causes a remarkable increase of N_2O concentration in both co-precipitation and impregnation catalysts. Some works propose that

N_2O formation is related to well-ordered MnO_X due to the presence of highly-reactive oxygen [28,~~49~~50], while other authors propose that N_2O is associated to Mn content in the catalysts (independently of structure and order) at high temperature [~~50~~51]. In this work, N_2O was found in all Mn-containing catalysts, with or without MnO_X crystals, and at temperatures above 150 ºC. Therefore, these results suggest that N_2O formation is largely associated to catalytic properties provided by Mn and not by its content or structure. In this regard, TPD experiments showed that the incorporation of Mn greatly increased the acid properties of the catalysts. Acid properties are strongly related to reactants oxidation on the catalyst surface; so, they could also be related to N_2O formation through the promotion of NH_3 oxidation.

Fig. 8

Regarding to N_2O production, similar N_2O profiles with two characteristic maxima are observed in co-precipitation and impregnation catalysts. In the case of impregnation catalysts, the two N_2O peaks are located at the same temperatures, 235 and 420 ºC, and the production is very similar, 140 and 123 ppm, respectively. For co-precipitation catalysts, N_2O production is higher than in impregnation catalysts in all temperature range. MnOx content above 50 mol.% produces a shift of N_2O production peaks from 245 and 421 ºC to 200 and 340 ºC, respectively. The fact that N_2O profiles are composed by two maxima may be associated to two chemical reactions, such as NH_3 oxidation and the non-selective reduction of NO, being involved in the formation of N_2O. The contribution of each reaction would depend on temperature.

Regarding to NO_2, this compound is formed at temperatures above 300 ºC, and its concentration continuously increases with temperature, which is in line with

the results of Want et al. [~~51~~52]. Pure CeO_2 in both series, 0Mn-100Ce and 0Mn/CeO_2, are the catalysts with the lowest NO_2 production. Mn-containing catalysts show a remarkable increase of NO_2 production, which slightly increases with Mn content in co-precipitation catalysts (around 300 ppm of NO_2 at 450 ºC, for catalysts above 80 mol.% MnO_X). Higher NO_2 production may be associated to the more oxidizing properties of co-precipitation catalysts due to better oxygen mobility and higher acidity. It should be noted the NO_2 production at temperatures below 300 ºC in impregnation catalysts. The same result is observed with co-precipitation 15Mn-85Ce catalyst. These facts reveal that Mn highly dispersed on CeO_2 promoted the formation of low amounts of NO_2 at low temperatures.

CO_2 and CO selectivity was calculated in order to carry out the by-products analysis in oxidation reaction. Fig. 9 shows the selectivity towards CO_2 of co-precipitation (Fig. 8A and 8B) and impregnation (Fig. 8C and 8D) catalysts from 200 ºC (below this temperature, some catalysts presented very low o-DCB conversion). CO_2 selectivity fits very well with o-DCB conversion results (Fig. 7). An increase of CO_2 selectivity is observed with Mn content in both~~,~~ co-precipitation and impregnation catalysts. Comparison between quantitative results obtained by the different preparation methods reveals that co-precipitation catalysts above 50 mol.% MnO_X promote, to a great extent, total oxidation of o-DCB, leading to CO_2 selectivity of 85 and 95% in the temperature ranges of 200-350 ºC and 350-450 ºC, respectively.

Fig. 9A and 9C show a drop in CO_2 selectivity at intermediate temperature. This drop is common in all samples containing both MnO_X and CeO_2, and coincides with the drop in o-DCB conversion (Fig. 7B and 7D). This fact may be

associated to a promotion of partial oxidation, which would favor the appearance of oxidation products other than CO_2. CO was the main by-product from oxidation reaction and its selectivity is show in Fig. 9B and 9D. In impregnation catalysts, except for $1Mn/CeO_2$, all catalysts containing both MnO_X and CeO_2 show selectivity to CO below 15% in all temperature range. On the other hand, co-precipitation catalysts promote selectivity to CO with Mn content at temperatures below 300 ºC. However, a drastic drop of selectivity to CO occurs at high temperature because of promotion of total oxidation of o-DCB. A slight increase in CO selectivity at intermediate temperatures, where CO_2 selectivity drops in both co-precipitation and impregnation catalysts with both MnO_X and CeO_2, should be noted. Moreover, the increase in CO selectivity is accompanied by the appearance of chlorinated by-products (Fig. 10). This fact corroborates that, under these conditions, o-DCB oxidation is promoted through partial oxidation, which has a negative effect in total oxidation.

Tetrachloroethylene and trichlorobenzene were the main chlorinated by-products identified in the temperature range of 275-420 ºC. The production of these compounds depends on Mn content. Thus, Fig. 10 shows that the formation of tetrachloroethylene in co-precipitation catalysts increases with Mn content, whereas trichlorobencene is promoted by high Ce contents. In the case of impregnation catalysts, trichlorobencene is the main by-product detected, because of the high Ce content, although traces of tetrachloroethylene are also detected in the impregnation catalysts with both MnO_X and CeO_2.

Fig. 10

Therefore, by-products formation and the slight increase of CO selectivity at intermediate temperature are in accordance with CO_2 selectivity decrease. This

fact, and the decrease of o-DCB conversion in the same temperature range, suggests a change in o-DCB oxidation pathway through partial oxidation reactions. According to literature, nucleophilic and electrophilic substitution through C-Cl bond is usually considered as the initial step of o-DCB oxidation, because of the weakness of this bond [~~52~~53]. However, at intermediate and high temperature, C-H bond in o-DCB becomes weaker because of the oxidizing power provided by Mn. So o-DCB could be also broken through other bonds of the molecule. This fact would evidence the coexistence of two pathways at medium-high temperature. In the first pathway, o-DCB would be oxidized through C-Cl bond, whereas in the second pathway o-DCB would be oxidized through C-H bond, promoting the appearance of chlorinated by products.

The appearance of the second pathway occurs at different temperature depending on oxidizing power of the catalysts. In this sense, Fig. 10 shows that chlorinated by-products are formed at lower temperature in co-precipitation catalysts. Characterization experiments showed that these catalysts presented better redox and acid properties, which improve their oxidizing performance. These results would be the reason why the high-temperature mechanism, evidenced by the appearance of chlorinated by-products, appears at lower temperature in co-precipitation catalysts.

3.2.3. Stability tests

Deactivation is an important aspect in the reactions involving catalytic oxidation of VOCs. In order to analyze the influence of Mn content and preparation method in deactivation, co-precipitation and impregnation catalysts with

different Mn contents were tested during 24 h in the simultaneous NO SCR and o-DCB oxidation at 300 ºC.

SCR results (Fig. 11A) show that NO conversion stabilized after 100 minutes in all catalysts. In co-precipitation catalysts, the trend in NO conversion differs depending on Mn content. In this way, the catalysts above 50 mol.% MnO_X show a decrease of NO conversion, so a clear deactivation of these catalysts occurs for SCR reaction. However, for 15Mn-85Ce, NO conversion increases initially. Stationary NO conversion is slightly higher in the catalysts with lower Mn content, and NO conversions of 88, 85 and 81% were obtained for 15Mn-85Ce, 50Mn-50Ce and 85Mn-15Ce, respectively. On the other hand, impregnation catalysts show similar results with final NO conversions of 88, 86 and 86% for 2Mn/CeO_2, 5Mn/CeO_2 and 8Mn/CeO_2, respectively. In this case, no initial deactivation of the catalysts was observed, NO conversion increasing up to the final values, as in the lowest-Mn-content co-precipitation catalyst. Stability results are in accordance with those from light-off experiments.

Fig. 11C shows the evolution of by-products in SCR stability tests. NO_2 and N_2O concentration decreases in 85Mn-15Ce and 8Mn/CeO_2 catalysts in the first 100 minutes of reaction. The fact that by-products concentration decreases in both catalysts in spite of the different trend observed in NO conversion refutes that Mn content affects SCR pathway and the side reactions involved in this process.

Fig. 11

Regarding to o-DCB oxidation (Fig. 11B), a clear deactivation is observed in the first 5 hours both in co-precipitation and impregnation catalysts. After this time, o-DCB conversion remains constant around 13% in impregnation catalysts,

whereas a smooth continuous decrease can be observed in co-precipitation catalysts, and o-DCB conversions of 70, 47 and 20% are obtained with 85Mn-15Ce, 50Mn-50Ce and 15Mn-85Ce, respectively, after 24 hours.

Concerning CO and CO_2 concentrations, Fig. 11D shows the evolution for 85Mn-15Ce and 8Mn/CeO_2 catalysts. The evolution of CO_2 is similar to that o-DCB conversion, with a strong initial decrease in both series. However, CO concentration increases, which indicates that deactivation affects not only o-DCB conversion, but also selectivity. The increase of CO concentration is accompanied by the appearance of chlorinated by-products (not shown) in the co-precipitation series. In the impregnation series, however, chlorinated by-products are not observed, probably because of the small o-DCB conversion.

Summarizing, both co-precipitation and impregnation catalysts undergo significant deactivation in o-DCB oxidation. In SCR, co-precipitation catalysts above 50 mol.% MnO_X are slightly deactivated as well. According to literature, no evidences of deactivation have been reported in SCR in the absence of o-DCB [21,~~36~~37]; thus, deactivation of the catalysts is probably strongly related to o-DCB oxidation. It is well known that oxidation of chlorinated compounds promotes deactivation effects in different types of catalysts at low temperature. Kan et al. associated the low-temperature deactivation of MnO_X-CeO_2 catalysts in the oxidation of chlorobenzene to the adsorption of Cl on the active sites [~~53~~54]. On the other hand, Hetrick et al. evidenced a strong contribution of surface carbonaceous deposits in deactivation of VO_X/TiO_2 catalysts in m-DCB oxidation [~~54~~55].

Table 4 summarizes chlorine and carbon content of used catalysts after stability tests. All catalysts show the presence of a high amount of chlorine and carbon

on the surface, which corroborates the presence of the deactivating species proposed in the literature. Wang et al. proposed that deactivation by chlorine occurs mainly in the CeO_2 surface, and the temperature from which Cl_2 is formed as a by-product depends on Mn content, decreasing with increasing Mn content [19]. These results are in line with the lower surface chlorine detected at higher Mn content in both co-precipitation and impregnation catalysts in Table 4, which reveals that this deactivating species is eliminated more easily from the surface when the amount of surface Mn is higher. However, no evidence of Cl_2 formation was observed in our experiments. This fact may be associated to the appearance of a white solid in the solid filter after the reactor, identified as ammonium chloride, which suggests that chlorine is removed by reaction with NH_3, one of the reactants in SCR. Easier removal of Cl at higher Mn content could be associated to weaker interaction of chlorine due to higher acidity and redox properties of the catalysts, taking into account the results of characterization.

Concerning carbon, co-precipitation catalysts present a surface carbon content decreasing with increasing Mn content. This result is probably associated to the improvement of oxygen species observed in XPS results, which favour removal of carbonaceous species through oxidation, generating carbon oxides. Impregnation catalysts present similar surface carbon content, which agrees with their observed similar performance in the process.

4. CONCLUSIONS

In this work, catalysts based in Mn and Ce were prepared by two methods, co-precipitation and impregnation, in order to study the effect of physicochemical properties and catalytic performance on the simultaneous reduction of NO and o-DCB oxidation. Characterization results showed that each preparation method favors different interaction between Mn and Ce. Thus, Mn is loaded on CeO_2 in impregnation catalysts, whereas Mn incorporates to the CeO_2 structure in co-precipitation catalysts, creating a solid solution. The formation of the solid solution plays an important role, because it enhances the redox properties through the generation of oxygen vacancies, which improve oxygen mobility. Moreover, an increase of acid properties is also provided by the high interaction between both metals.

The catalytic tests have corroborated the better activity of catalysts prepared by co-precipitation, with increased NO and o-DCB conversion at low temperature compared to impregnation catalysts. In this way, catalysts above 80 mol.% MnO_X showed the best catalytic activity, with NO conversions above 90% at temperatures below 250 ºC and o-DCB conversions above 80% at temperatures above 200 ºC. In these catalysts, XRD and TPR evidenced coexistence of Mn_2O_3 crystals and the solid solution, which could be responsible for the great catalytic performance. Regarding to selectivity, N_2O and NO_2 were the main by-products of SCR reaction in both impregnation and co-precipitation catalysts. N_2O is produced in all temperature range, whereas NO_2 is observed above 300 ºC. The formation of these compounds is favored by the improvement of oxidation properties, which are clearly related to Mn species. In oxidation reaction, co-precipitation catalysts present slightly higher

selectivity to CO_2, above 80%. However, an increase of selectivity to CO and chlorinated by-products production at medium temperature evidenced a possible change in the oxidation pathway, in which higher amount of oxidation intermediates is involved. Stability tests evidenced deactivation in all catalysts, mainly in the oxidation reaction. Deactivation is affected by preparation method and Mn content in co-precipitation catalysts and is associated to Cl adsorption, which is also detrimental for total oxidation of o-DCB.

5. ACKNOWLEDGMENTS

The authors thank MINECO/FEDER (CTQ2015-64616-P), The Basque Government (IT657-13 and IT1297-19) and the University of the Basque Country UPV/EHU (INF12/37, UFI 11/39) for the economic support. The author JAMM specially acknowledges MINECO/FEDER (BES-2016-077849) for the PhD grant. Likewise, the authors thank technical and human support provided by SGIker of UPV/EHU and European funding (ERDF and ESF).

REFERENCES

[1] M. Goemans, P. Clarysse, J. Joannès, P. De Clercq, S. Lenaerts, K. Matthys, K. Boels, Catalytic NO_X reduction with simultaneous dioxin and furan oxidation,50 (2003) 489-497.
https://doi.org/10.1016/S0045-6535(02)00554-4.

[2] E. Finocchio, G. Busca, M. Notaro, A review of catalytic processes for the destruction of PCDD and PCDF from waste gases, Appl. Catal. B Environ. 62 (2006) 12-20.
https://doi.org/10.1016/j.apcatb.2005.06.010.

[3] G. Qi, R.T. Yang, Low-temperature selective catalytic reduction of NO with NH_3 over iron and manganese oxides supported on titania, Appl. Catal. B Environ. 44 (2003) 217-225.
https://doi.org/10.1016/S0926-3373(03)00100-0.

[4] F. Gao, X. Tang, H. Yi, S. Zhao, C. Li, J. Li, Y. Shi, X. Meng, A review on selective catalytic reduction of NO_X by NH_3 over Mn–based catalysts at low temperatures: Catalysts, mechanisms, kinetics and DFT calculations, Catalysts 7 (2017).
https://doi.org/10.3390/catal7070199.

[5] M. Gallastegi-Villa, A. Aranzabal, Z. Boukha, J.A. González-Marcos, J.R. González-Velasco, M.V. Martínez-Huerta, M.A. Bañares, Role of surface vanadium oxide coverage support on titania for the simultaneous removal of o-dichlorobenzene and NO_x from waste incinerator flue gas, Catal Today. 254 (2015) 2-11.
https://doi.org/10.1016/j.cattod.2015.02.029.

[6] S. Zhang, B. Zhang, B. Liu, S. Sun, A review of Mn-containing oxide catalysts for low temperature selective catalytic reduction of NO_X with NH_3: Reaction mechanism and catalyst deactivation, RSC Adv. 7 (2017) 26226-26242.
https://doi.org/10.1039/c7ra03387g.

[7] R. Jin, Y. Liu, Z. Wu, H. Wang, T. Gu, Low-temperature selective catalytic reduction of NO with NH_3 over Mn-Ce oxides supported on TiO_2 and Al_2O_3 : A comparative study, Chemosphere 78 (2010) 1160-1166.
https://doi.org/10.1016/j.chemosphere.2009.11.049.

[8] K. Qi, J. Xie, Z. Zhang, D. Fang, D. Han, X. Liu, P. Gong, F. Li, F. He, Facile large-scale synthesis of Ce–Mn composites by redox-precipitation and its superior low-temperature performance for NO removal, Powder Technol. 338 (2018) 774-782.
https://doi.org/10.1016/j.powtec.2018.07.073.

[9] B. Thirupathi, P.G. Smirniotis, Co-doping a metal (Cr, Fe, Co, Ni, Cu, Zn, Ce, and Zr) on Mn/TiO_2 catalyst and its effect on the selective reduction of NO with NH_3 at low-temperatures, Appl. Catal. B Environ. 110 (2011) 195-206.

https://doi.org/10.1016/j.apcatb.2011.09.001.

[10] X. Wang, L. Zhang, S. Wu, W. Zou, S. Yu, Y. Shao, L. Dong, Promotional effect of Ce on iron-based catalysts for selective catalytic reduction of NO with NH_3, Catalysts 6 (2016).
https://doi.org/10.3390/catal6080112.

[11] Y. Wan, W. Zhao, Y. Tang, L. Li, H. Wang, Y. Cui, J. Gu, Y. Li, J. Shi, Ni-Mn bi-metal oxide catalysts for the low temperature SCR removal of NO with NH_3, Appl. Catal. B Environ. 148-149 (2014) 114-122.
https://doi.org/10.1016/j.apcatb.2013.10.049.

[12] M. Kang, T.H. Yeon, E.D. Park, J.E. Yie, J.M. Kim, Novel MnO_X catalysts for NO reduction at low temperature with ammonia, Catal Lett. 106 (2006) 77-80.
https://doi.org/10.1007/s10562-005-9194-3.

[13] J. Li, J. Chen, R. Ke, C. Luo, J. Hao, Effects of precursors on the surface Mn species and the activities for NO reduction over MnO_X/TiO_2 catalysts, Catal. Commun. 8 (2007) 1896-1900.
https://doi.org/10.1016/j.catcom.2007.03.007.

[14] V.P. Santos, M.F.R. Pereira, J.J.M. Órfão, J.L. Figueiredo, The role of lattice oxygen on the activity of manganese oxides towards the oxidation of volatile organic compounds, Appl. Catal. B Environ. 99 (2010) 353-363.
https://doi.org/10.1016/j.apcatb.2010.07.007.

[15] Z. Liu, Y. Yi, S. Zhang, T. Zhu, J. Zhu, J. Wang, Selective catalytic reduction of NO_X with NH_3 over Mn-Ce mixed oxide catalyst at low temperatures, Catal Today. 216 (2013) 76-81.
https://doi.org/10.1016/j.cattod.2013.06.009.

[16] G. Qi, R.T. Yang, R. Chang, MnO_X-CeO_2 mixed oxides prepared by co-precipitation for selective catalytic reduction of NO with NH_3 at low temperatures, Appl. Catal. B Environ. 51 (2004) 93-106.
https://doi.org/10.1016/j.apcatb.2004.01.023.

[17] B. Shen, X. Zhang, H. Ma, Y. Yao, T. Liu, A comparative study of Mn/CeO_2, Mn/ZrO_2 and Mn/Ce-ZrO_2 for low temperature selective catalytic reduction of NO with NH_3 in the presence of SO_2 and H_2O, J. Environ. Sci. 25 (2013) 791-800.
https://doi.org/10.1016/S1001-0742(12)60109-0.

[18] X. Wang, L. Ran, Y. Dai, Y. Lu, Q. Dai, Removal of Cl adsorbed on Mn-Ce-La solid solution catalysts during CVOC combustion, J. Colloid Interface Sci. 426 (2014) 324-332.
https://doi.org/10.1016/j.jcis.2013.10.007.

[19] W. Xingyi, K. Qian, L. Dao, Catalytic combustion of chlorobenzene over MnO_X-CeO_2 mixed oxide catalysts, Appl. Catal. B Environ. 86 (2009) 166-175.

https://doi.org/10.1016/j.apcatb.2008.08.009.

[20] Y. Wu, Y. Zhang, M. Liu, Z. Ma, Complete catalytic oxidation of o-xylene over Mn-Ce oxides prepared using a redox-precipitation method, Catal Today. 153 (2010) 170-175.
https://doi.org/10.1016/j.cattod.2010.01.064.

[21] X. Yao, K. Ma, W. Zou, S. He, J. An, F. Yang, L. Dong, Influence of preparation methods on the physicochemical properties and catalytic performance of MnO_X-CeO_2 catalysts for NH_3-SCR at low temperature, Cuihua Xuebao Chin. J. Catalysis. 38 (2017) 146-159.
https://doi.org/10.1016/S1872-2067(16)62572-X.

[22] B. Shen, F. Wang, T. Liu, Homogeneous MnO_X-CeO_2 pellets prepared by a one-step hydrolysis process for low-temperature NH_3-SCR, Powder Technol. 253 (2014) 152-157.
https://doi.org/10.1016/j.powtec.2013.11.015.

[23] G. Picasso, M. Gutiérrez, M.P. Pina, J. Herguido, Preparation and characterization of Ce-Zr and Ce-Mn based oxides for n-hexane combustion: Application to catalytic membrane reactors, Chem. Eng. J. 126 (2007) 119-130.
https://doi.org/10.1016/j.cej.2006.09.005.

[24] Q. Shen, L. Zhang, N. Sun, H. Wang, L. Zhong, C. He, W. Wei, Y. Sun, Hollow MnO_X-CeO_2 mixed oxides as highly efficient catalysts in NO oxidation, Chem. Eng. J. 322 (2017) 46-55.
https://doi.org/10.1016/j.cej.2017.02.148.

[25] S. Ramana, B.G. Rao, P. Venkataswamy, A. Rangaswamy, B.M. Reddy, Nanostructured Mn-doped ceria solid solutions for efficient oxidation of vanillyl alcohol, J. Mol. Catal. A Chem. 415 (2016) 113-121.
https://doi.org/10.1016/j.molcata.2016.01.028.

[26] X. Wu, Q. Liang, D. Weng, J. Fan, R. Ran, Synthesis of CeO_2-MnO_X mixed oxides and catalytic performance under oxygen-rich condition, Catal Today. 126 (2007) 430-435.
https://doi.org/10.1016/j.cattod.2007.06.014.

[27] X. Wu, F. Lin, H. Xu, D. Weng, Effects of adsorbed and gaseous NO_X species on catalytic oxidation of diesel soot with MnO_X-CeO_2 mixed oxides, Appl. Catal. B Environ. 96 (2010) 101-109.
https://doi.org/10.1016/j.apcatb.2010.02.006.

[28] X. Tang, Y. Li, X. Huang, Y. Xu, H. Zhu, J. Wang, W. Shen, MnO_X-CeO_2 mixed oxide catalysts for complete oxidation of formaldehyde: Effect of preparation method and calcination temperature, Appl. Catal. B Environ. 62 (2006) 265-273.
https://doi.org/10.1016/j.apcatb.2005.08.004.

[29] F. Bertinchamps, C. Grégoire, E.M. Gaigneaux, Systematic investigation of supported transition metal oxide based formulations for the catalytic oxidative elimination of (chloro)-aromatics. Part I: Identification of the optimal main active phases and supports, Appl. Catal. B Environ. 66 (2006) 1-9. https://doi.org/10.1016/j.apcatb.2006.02.011.

[~~29~~30] M.A. Larrubia, G. Busca, An FT-IR study of the conversion of 2-chloropropane, o-dichlorobenzene and dibenzofuran on V_2O_5 -MoO_3-TiO_2 SCR-deNO_X catalysts, Appl. Catal. B Environ. 39 (2002) 343-352. https://doi.org/10.1016/S0926-3373(02)00116-9.

[~~30~~31] S. Albonetti, S. Blasioli, R. Bonelli, J.E. Mengou, S. Scirè, F. Trifirò, The role of acidity in the decomposition of 1,2-dichlorobenzene over TiO_2-based V_2O_5/WO_3 catalysts, Appl Catal A Gen. 341 (2008) 18-25. https://doi.org/10.1016/j.apcata.2007.12.033.

[~~31~~32] H. Li, G. Lu, Q. Dai, Y. Wang, Y. Guo, Y. Guo, Efficient low-temperature catalytic combustion of trichloroethylene over flower-like mesoporous Mn-doped CeO_2 microspheres, Appl. Catal. B Environ. 102 (2011) 475-483. https://doi.org/10.1016/j.apcatb.2010.12.029.

[~~32~~33] Q. Ye, B.-. Xu, Textural and structure characterizations of $Ce_{1-X}Mn_XO_2$ prepared by citric acid sol-gel method, Acta Phys. Chim. Sin. 22 (2006) 345-349. https://doi.org/10.3866/PKU.WHXB20060318.

[~~33~~34] X. Du, D. Zhang, L. Shi, R. Gao, J. Zhang, Morphology dependence of catalytic properties of Ni/CeO_2 nanostructures for carbon dioxide reforming of methane, J. Phys. Chem. C. 116 (2012) 10009-10016. https://doi.org/10.1021/jp300543r.

[~~34~~35] C. Tang, J. Li, X. Yao, J. Sun, Y. Cao, L. Zhang, F. Gao, Y. Deng, L. Dong, Mesoporous NiO-CeO_2 catalysts for CO oxidation: Nickel content effect and mechanism aspect, Appl Catal A Gen. 494 (2015) 77-86. https://doi.org/10.1016/j.apcata.2015.01.037.

[~~35~~36] P. Venkataswamy, D. Jampaiah, C.U. Aniz, B.M. Reddy, Investigation of physicochemical properties and catalytic activity of nanostructured $Ce_{0.7}M_{0.3}O_2$ (M = Mn, Fe, Co) solid solutions for CO oxidation, J. Chem. Sci. 127 (2015) 1347-1360. https://doi.org/10.1007/s12039-015-0897-8.

[~~36~~37] X. You, Z. Sheng, D. Yu, L. Yang, X. Xiao, S. Wang, Influence of Mn/Ce ratio on the physicochemical properties and catalytic performance of graphene supported MnO_X-CeO_2 oxides for NH_3-SCR at low temperature, Appl. Surf. Sci. 423 (2017) 845-854. https://doi.org/10.1016/j.apsusc.2017.06.226.

[~~37~~38] C.M. Julien, M. Massot, C. Poinsignon, Lattice vibrations of manganese oxides: Part I. Periodic structures, Spectrochim. Acta Part A Mol. Biomol. Spectrosc. 60 (2004) 689-700. https://doi.org/10.1016/S1386-1425(03)00279-8.

[~~38~~39] H. Chen, A. Sayari, A. Adnot, F. Larachi, Composition-activity effects of Mn-Ce-O composites on phenol catalytic wet oxidation, Appl. Catal. B Environ. 32 (2001) 195-204. https://doi.org/10.1016/S0926-3373(01)00136-9.

[~~39~~40] X. Tang, J. Li, L. Sun, J. Hao, Origination of N_2O from NO reduction by NH_3 over β-MnO_2 and α-Mn_2O_3, Appl. Catal. B Environ. 99 (2010) 156-162. https://doi.org/https://doi.org/10.1016/j.apcatb.2010.06.012.

[~~40~~41] E.R. Stobbe, B.A. De Boer, J.W. Geus, The reduction and oxidation behaviour of manganese oxides, Catal Today. 47 (1999) 161-167. https://doi.org/10.1016/S0920-5861(98)00296-X.

[~~41~~42] Z. Wu, N. Tang, L. Xiao, Y. Liu, H. Wang, MnO_X/TiO_2 composite nanoxides synthesized by deposition-precipitation method as a superior catalyst for NO oxidation, J. Colloid Interface Sci. 352 (2010) 143-148. https://doi.org/10.1016/j.jcis.2010.08.031.

[~~42~~43] Y. Wang, X. Li, L. Zhan, C. Li, W. Qiao, L. Ling, Effect of SO_2 on activated carbon honeycomb supported CeO_2-MnO_X catalyst for NO removal at low temperature, Ind Eng Chem Res. 54 (2015) 2274-2278. https://doi.org/10.1021/ie504074h.

[~~43~~44] M.D.H. Chowdhury, J.G. Um, J. Jang, Remarkable changes in interface O vacancy and metal-oxide bonds in amorphous indium-gallium-zinc-oxide thin-film transistors by long time annealing at 250 °C, Appl. Phys. Lett. 105 (2014). https://doi.org/10.1063/1.4903874.

[~~44~~45] C. Bozo, N. Guilhaume, J. Herrmann, Role of the ceria-zirconia support in the reactivity of platinum and palladium catalysts for methane total oxidation under lean conditions, J. Catal. 203 (2001) 393-406. https://doi.org/10.1006/jcat.2001.3320.

[~~45~~46] S. Ponce, M.A. Peña, J.L.G. Fierro, Surface properties and catalytic performance in methane combustion of SR-substituted lanthanum manganites, Appl. Catal. B Environ. 24 (2000) 193-205. https://doi.org/10.1016/S0926-3373(99)00111-3.

[~~46~~47] J. Chen, M. Shen, X. Wang, G. Qi, J. Wang, W. Li, The influence of nonstoichiometry on $LaMnO_3$ perovskite for catalytic NO oxidation, Appl. Catal. B Environ. 134-135 (2013) 251-257. https://doi.org/10.1016/j.apcatb.2013.01.027.

[4748] Y. Dai, X. Wang, Q. Dai, D. Li, Effect of Ce and La on the structure and activity of MnO_X catalyst in catalytic combustion of chlorobenzene, Appl. Catal. B Environ. 111-112 (2012) 141-149. https://doi.org/10.1016/j.apcatb.2011.09.028.

[4849] S. Ren, J. Yang, T. Zhang, L. Jiang, H. Long, F. Guo, M. Kong, Role of cerium in improving NO reduction with NH_3 over Mn–Ce/ASC catalyst in low-temperature flue gas, Chem. Eng. Res. Des. 133 (2018) 1-10. https://doi.org/10.1016/j.cherd.2018.02.041.

[4950] T.S. Park, S.K. Jeong, S.H. Hong, S.C. Hong, Selective catalytic reduction of nitrogen oxides with NH_3 over natural manganese ore at low temperature, Ind Eng Chem Res. 40 (2001) 4491-4495. https://doi.org/10.1021/ie010218.

[5051] M. Kang, E.D. Park, J.M. Kim, J.E. Yie, Manganese oxide catalysts for NO_X reduction with NH_3 at low temperatures, Appl Catal A Gen. 327 (2007) 261-269. https://doi.org/10.1016/j.apcata.2007.05.024.

[5152] C. Wang, F. Yu, M. Zhu, C. Tang, K. Zhang, D. Zhao, L. Dong, B. Dai, Highly selective catalytic reduction of NO_X by MnO_X–CeO_2–Al_2O_3 catalysts prepared by self-propagating high-temperature synthesis, J. Environ. Sci. 75 (2019) 124-135. https://doi.org/10.1016/j.jes.2018.03.011.

[5253] J. Lichtenberger, M.D. Amiridis, Catalytic oxidation of chlorinated benzenes over V_2O_5/TiO_2 catalysts, J. Catal. 223 (2004) 296-308. https://doi.org/10.1016/j.jcat.2004.01.032.

[5354] J. Kan, L. Deng, B. Li, Q. Huang, S. Zhu, S. Shen, Y. Chen, Performance of co-doped Mn-Ce catalysts supported on cordierite for low concentration chlorobenzene oxidation, Appl Catal A Gen. 530 (2017) 21-29. https://doi.org/10.1016/j.apcata.2016.11.013.

[5455] C.E. Hetrick, F. Patcas, M.D. Amiridis, Effect of water on the oxidation of dichlorobenzene over V_2O_5/TiO_2 catalysts, Appl. Catal. B Environ. 101 (2011) 622-628. https://doi.org/10.1016/j.apcatb.2010.11.003.

TABLE AND FIGURE CAPTIONS

Table 1: Textural properties of the catalysts.

Table 2: Redox and acidic properties of the catalysts.

Table 3: XPS results of catalysts. Binding energies and surface atomic relations.

Table 4: Chlorine and carbon contents of used catalysts after stability tests.

Fig. 1: Experimental set-up.

Fig. 2: XRD patterns of A) co-precipitation catalysts and B) impregnation catalysts.

Fig. 3: Raman spectra of A) co-precipitation catalysts and B) impregnation catalysts.

Fig. 4: TPR profiles of A) co-precipitation catalysts and B) impregnation catalysts.

Fig. 5: XPS spectra of co-precipitation catalysts: A) Ce 3d 5/2 C) Mn 2p E) O 1s; and impregnation catalysts: B) Ce 3d 5/2 D) Mn 2p F) O 1s.

Fig. 6: NH_3-TPD profiles of A) Co-precipitation catalysts and B) impregnation catalysts.

Fig. 7: Catalytic activity of co-precipitation catalysts: A) NO conversion and C) o-DCB conversion; and impregnation catalysts B) NO conversion and D) o-DCB conversion. Gas composition: 100 ppm o-DCB, 300 ppm NO, 300 ppm NH_3 and 10% O_2 at 1.5 atm 2 L_N min^{-1} and 60 L_N $(h \cdot g)^{-1}$.

Fig. 8: N_2O concentration of A) co-precipitation catalysts C) impregnation catalysts; NO_2 concentration B) co-precipitation catalysts D) impregnation catalysts.

Fig. 9: CO_2 selectivity of A) co-precipitation catalysts C) impregnation catalysts; CO selectivity B) co-precipitation catalysts D) impregnation catalysts.

Fig. 10: Chlorinated by-products produced in o-DCB oxidation reaction by co-precipitation catalysts A) Tetrachloroethylene B) Trichlorobenzene; and impregnation catalysts C) Tetrachloroethylene D) Trichlorobenzene.

Fig. 11: Stability test of co-precipitation and impregnation Mn-contain catalysts at 300 ºC. Gas composition: 100 ppm o-DCB, 300 ppm NO, 300 ppm NH_3 and 10% O_2 at 1.5 atm, 2 L_N min^{-1} and 60 L_N $(h \cdot g)^{-1}$. A) NO conversions B) o-DCB conversions C) N_2O and NO_2 concentrations D) CO_2 and CO concentrations.

Table 1

1 Table 1

Sample	S_{BET} (m^2/g)	V_p (cm^3/g)	Lattice parameter (Å)	Fluorite crystal size (nm)	MnO_X[a] crystal size (nm)
0Mn-100Ce	80.4	0.11	5.4135	8.7	--
15Mn-85Ce	84.4	0.18	5.4054	5.1	--
50Mn-50Ce	88.3	0.21	5.4035	4.4	--
80Mn-20Ce	84.3	0.25	5.4023	4.5	14.7
85Mn-15Ce	87.1	0.25	5.4107	4.5	17.5
90Mn-10Ce	98.8	0.25	5.4071	4.6	19.1
100Mn-0Ce	34.4	0.19	--	--	21.5
0Mn/CeO_2	67.1	0.13	5.4169	8.7	--
1Mn/CeO_2	59.9	0.16	5.4159	8.3	--
2Mn/CeO_2	63.1	0.17	5.4161	8.2	--
3Mn/CeO_2	55.3	0.16	5.4166	8.4	--
5Mn/CeO_2	54.5	0.14	5.4151	8.2	--
8Mn/CeO_2	48.1	0.13	5.4146	8.3	--
MnO_X	1.9	0.01	--	--	9.45

2 a: Mn_2O_3 for co-precipitated catalysts and MnO_2 for impregnated catalysts.

Table 2

1 Table 2

Sample	H_2 consumption (mmol H_2/g)	Mn oxidation state	Bulk proportion Mn^{3+}/Mn^{4+}	Acidity (μmol NH_3/g)			Acidity (μmol NH_3/m^2)
				Weak	Strong	Total	Total
0Mn-100Ce	1.34	--	--/--	95.8	108.7	204.1	2.5
15Mn-85Ce	1.67	4.01	0.0/1.0	88.6	152.7	241.3	2.9
50Mn-50Ce	3.05	3.45	0.55/0.45	102.7	201.7	304.5	3.4
80Mn-20Ce	4.94	3.27	0.73/0.27	121.6	159.6	281.2	3.3
85Mn-15Ce	5.29	3.22	0.78/0.22	128.6	170.8	299.4	3.4
90Mn-10Ce	5.86	3.32	0.68/0.32	150.9	207.6	358.5	3.6
100Mn-0Ce	6.59	3.09	0.91/0.09	81.4	89.7	171.0	5.0
$0Mn/CeO_2$	1.20	--	--/--	78.5	48.4	126.9	1.9
$1Mn/CeO_2$	0.88	--	--/--	68.4	79.1	147.5	2.4
$2Mn/CeO_2$	1.30	2.81	--/--	60.0	100.2	160.2	2.5
$3Mn/CeO_2$	1.30	3.22	*0.78/0.22*	58.1	110.4	168.5	3.0
$5Mn/CeO_2$	2.00	3.94	0.06/0.94	60.1	108.1	168.2	3.1
$8Mn/CeO_2$	2.40	3.67	0.33/0.67	51.0	70.8	121.8	2.5
MnO_X	7.00	3.12	0.88/0.12	7.4	3.3	10.7	5.6

2

Table 3

Table 3

Sample	Mn 2p 3/2 BE (eV)		Surface proportion Mn^{3+}/Mn^{4+}	Surface proportion Ce^{3+}/Ce^{4+}	$O^{II}/(O^{I} + O^{II} + O^{III})$
	Mn^{4+}	Mn^{3+}			
0Mn-100Ce	--	--	--/--	--/--	--
15Mn-85Ce	642.2	640.8	0.55/0.45	0.14/0.86	0.24
50Mn-50Ce	642.2	640.8	0.54/0.46	0.15/0.85	0.28
80Mn-20Ce	642.3	641.0	0.54/0.46	0.16/0.84	0.33
85Mn-15Ce	642.3	641.1	0.57/0.43	0.13/0.87	0.34
90Mn-10Ce	642.4	641.2	0.56/0.44	0.16/0.84	0.35
100Mn-0Ce	642.1	640.8	0.54/0.46	--/--	0.28
$0Mn/CeO_2$	--	--	--/--	--/--	--
$1Mn/CeO_2$	642.2	640.9	0.63/0.37	0.19/0.81	--
$2Mn/CeO_2$	642.5	641.0	0.57/0.43	0.17/0.83	--
$3Mn/CeO_2$	642.4	640.8	0.57/0.43	0.17/0.83	--
$5Mn/CeO_2$	642.4	640.9	0.61/0.39	0.18/0.82	--
$8Mn/CeO_2$	642.4	641.0	0.59/0.41	0.19/0.81	--
MnO_X	642.3	641.1	0.49/0.51	--/--	--

Table 4

1 Table 4

Sample	Cl (wt. %)	C (wt. %)
15Mn-85Ce	2.60	6.37
50Mn-50Ce	2.11	5.42
85Mn-15Ce	1.76	4.87
1Mn/CeO_2	1.52	4.26
3Mn/CeO_2	1.47	4.93
5Mn/CeO_2	1.22	4.49

2

Figure 1

Click here to download high resolution image

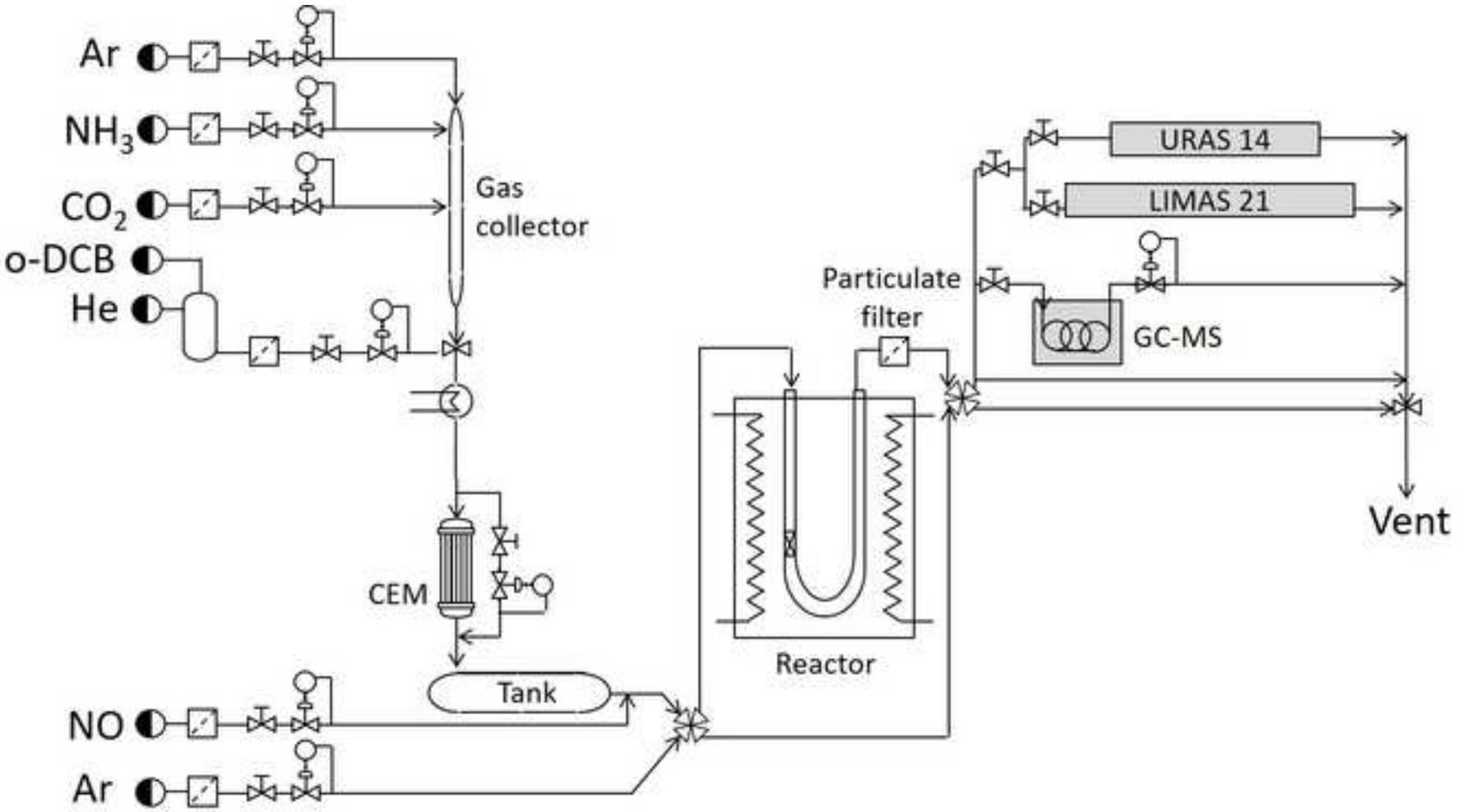

Figure 2

Click here to download high resolution image

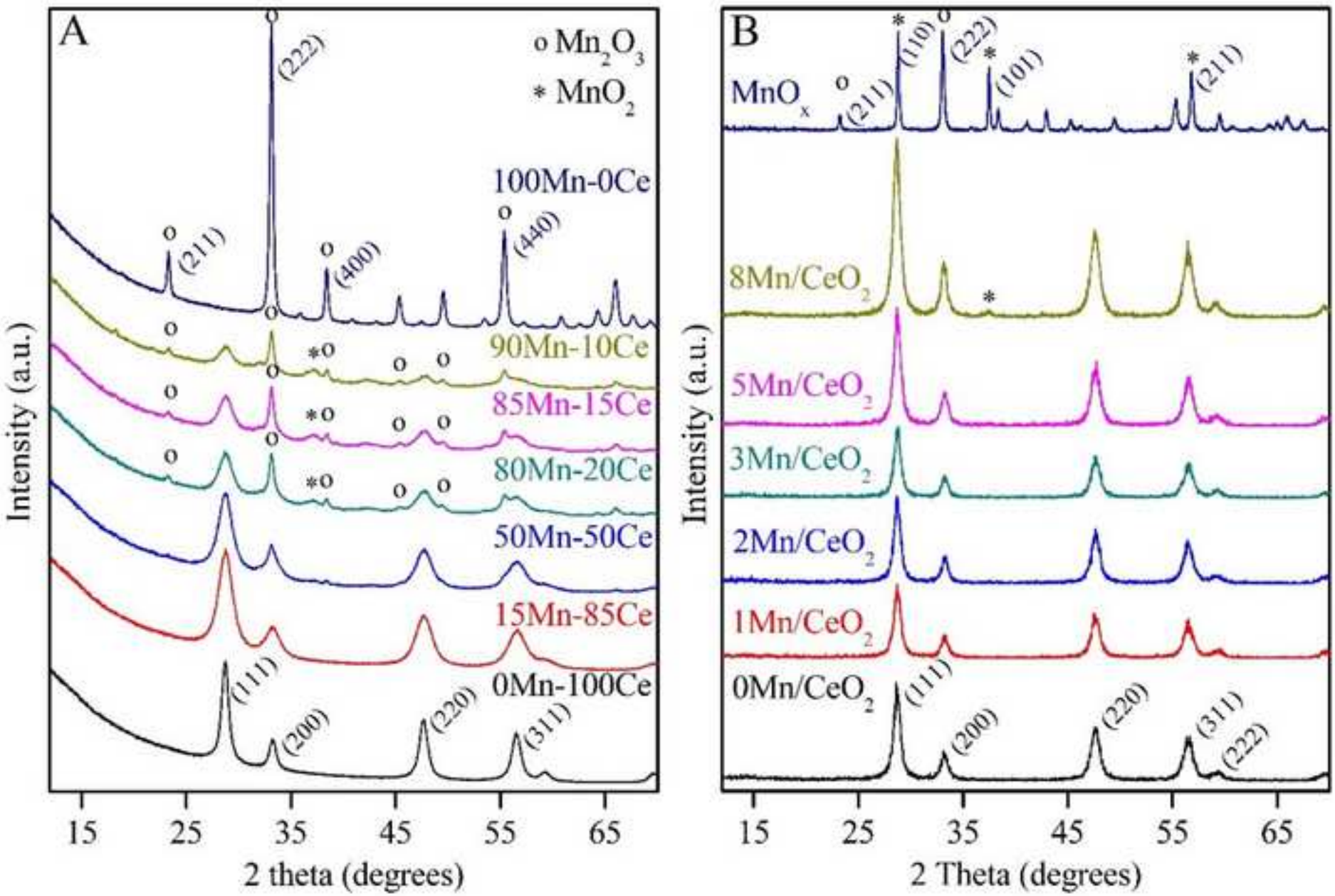

Figure 3

Click here to download high resolution image

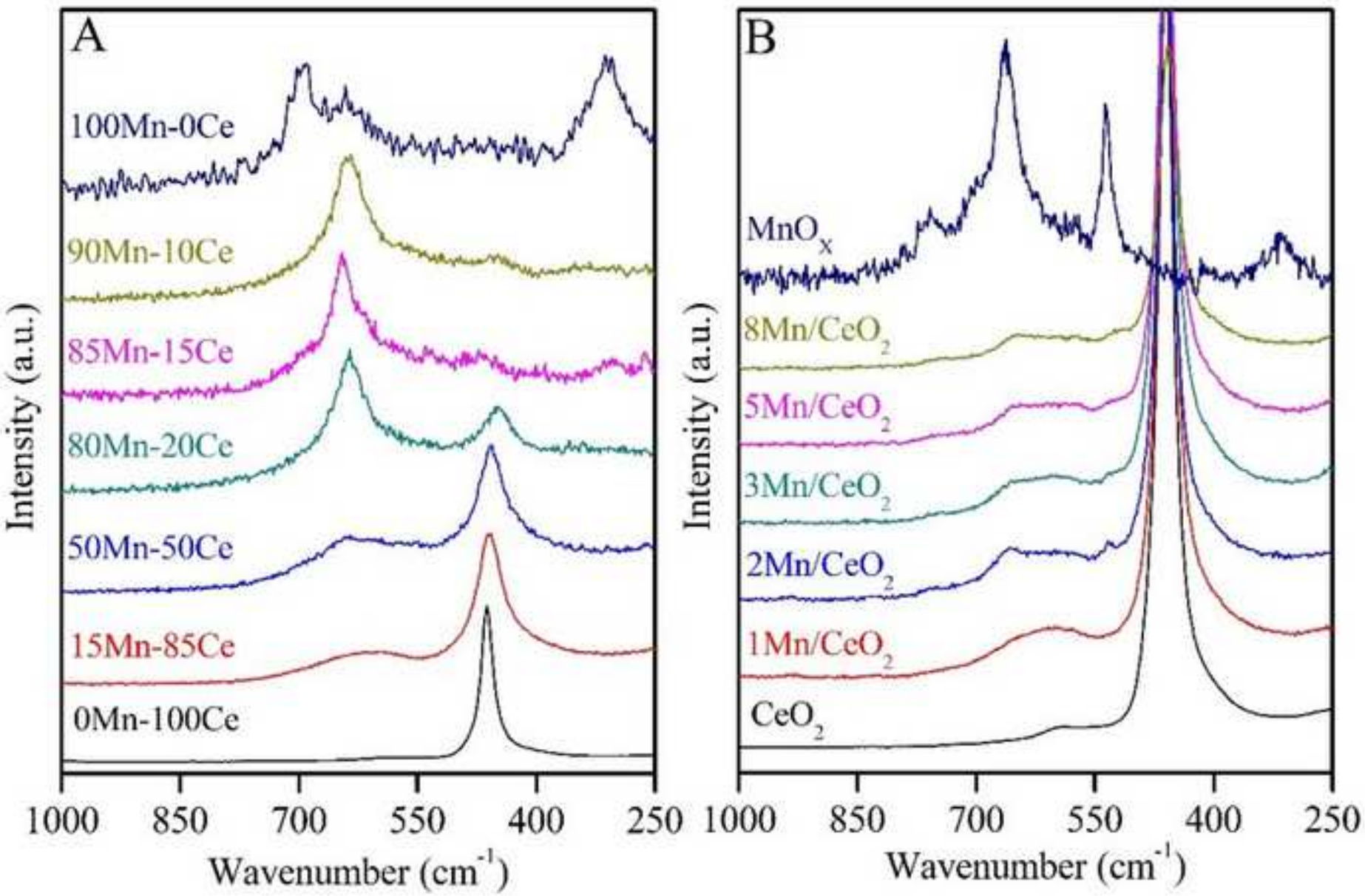

Figure 4

Click here to download high resolution image

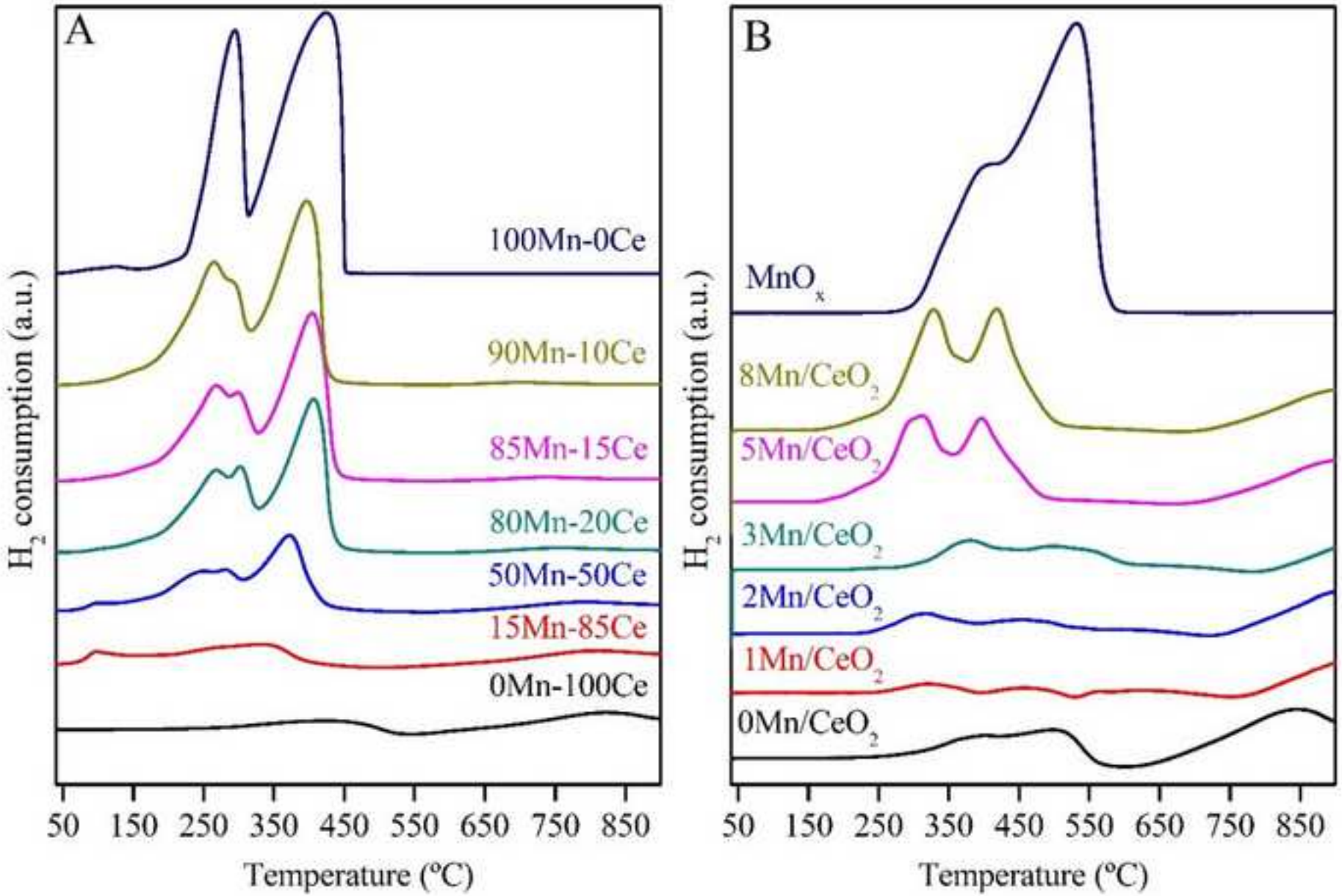

Figure 5

Click here to download high resolution image

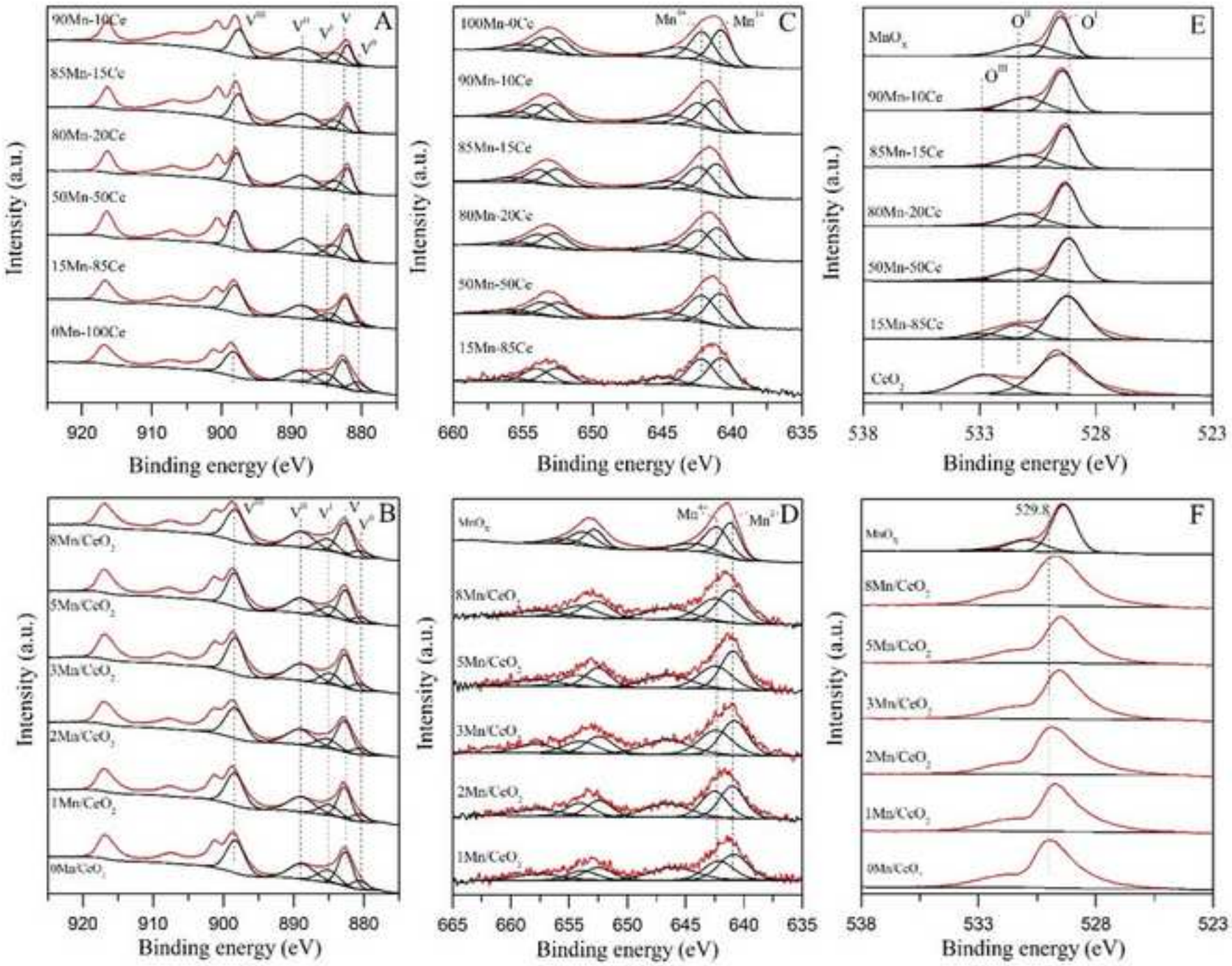

Figure 6

Click here to download high resolution image

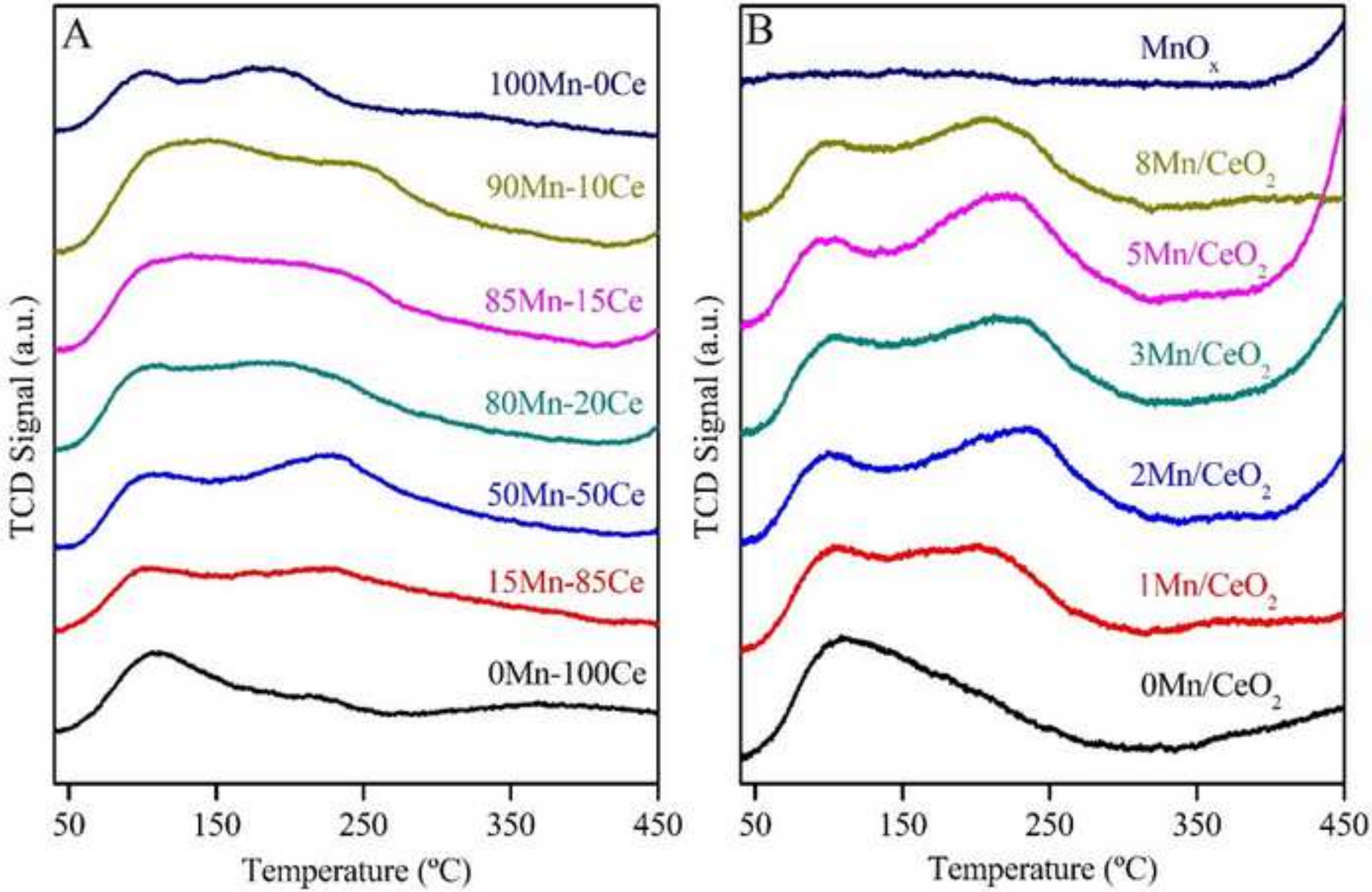

Figure 7

Click here to download high resolution image

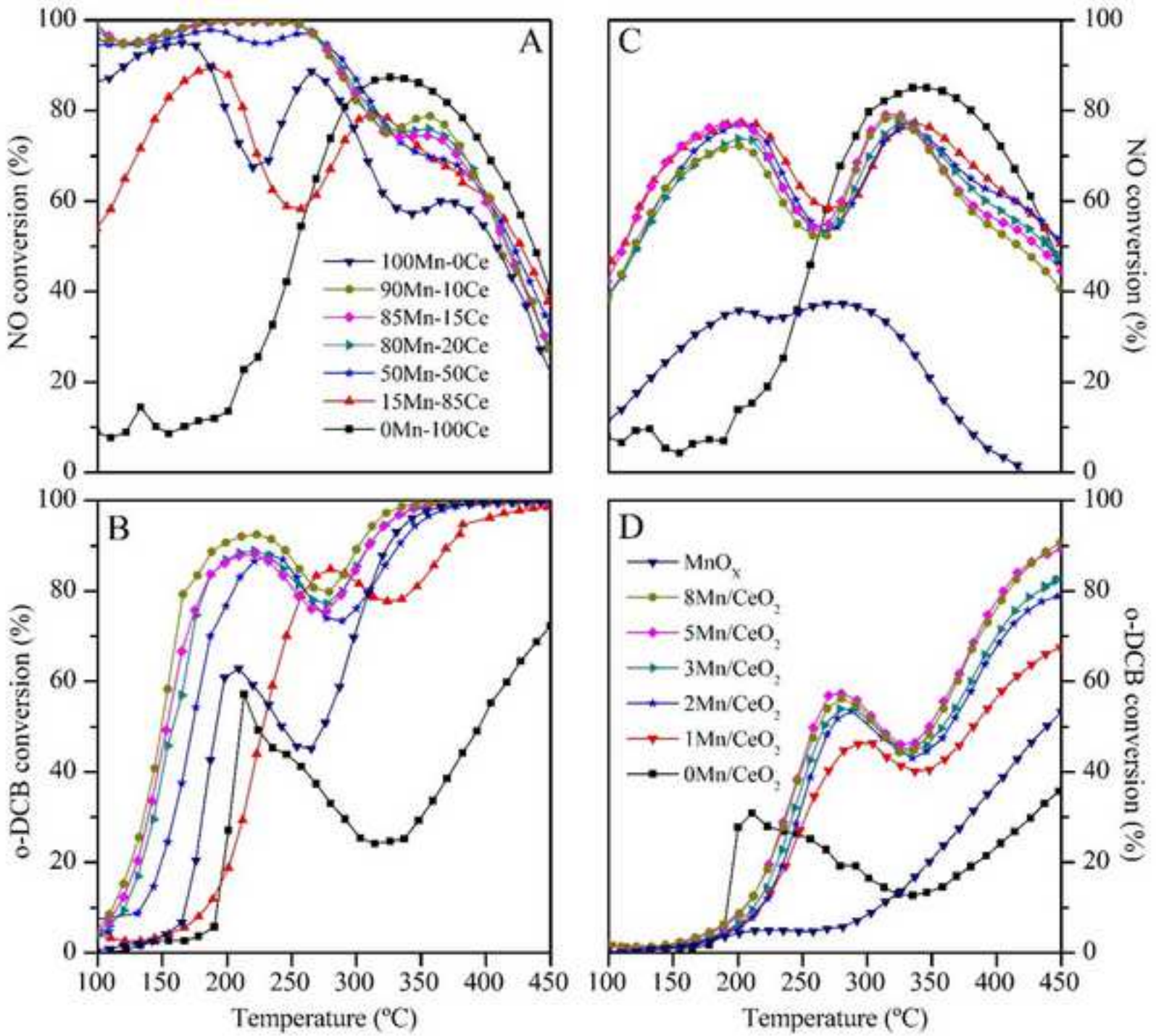

Figure 8

Click here to download high resolution image

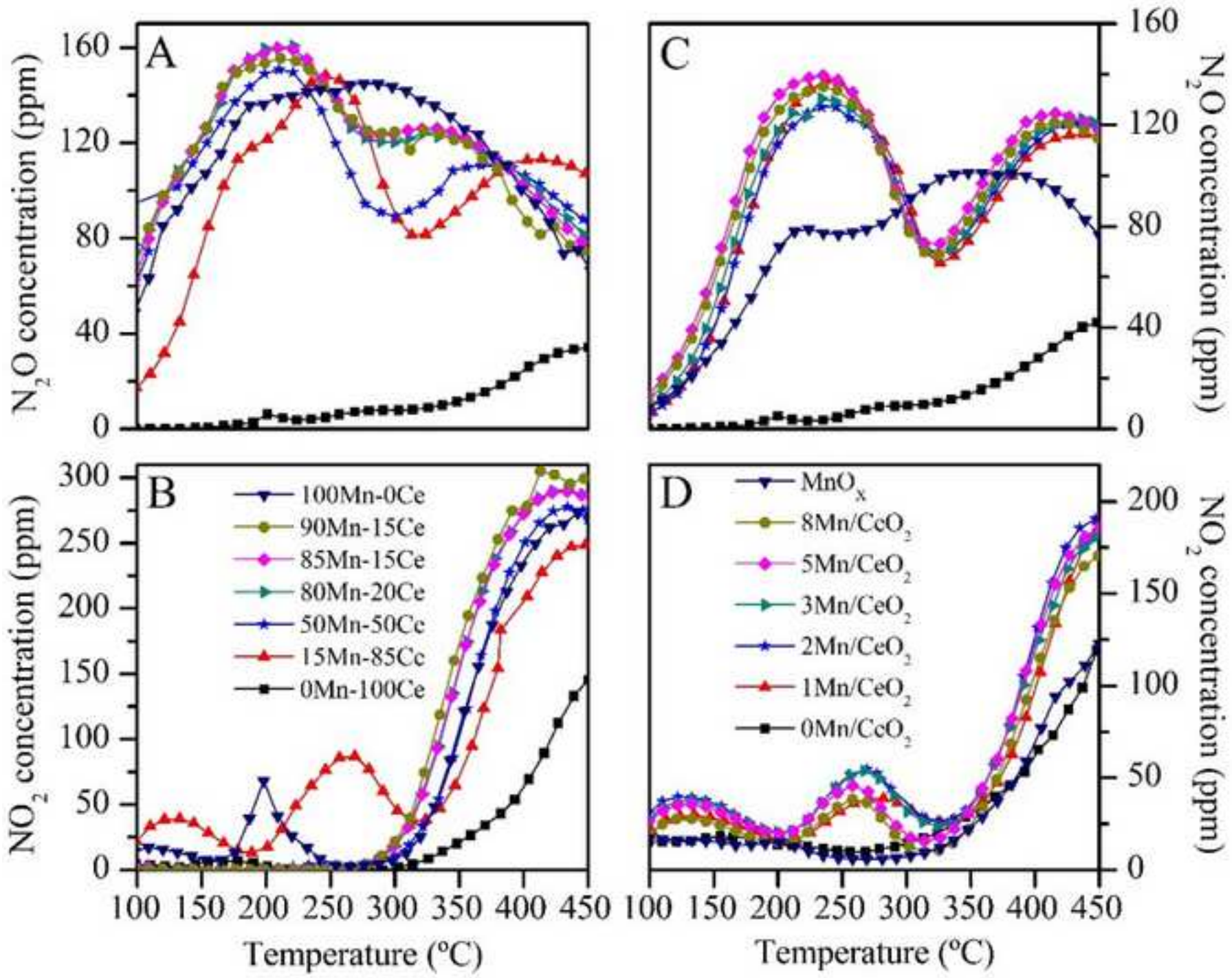

Figure 9

Click here to download high resolution image

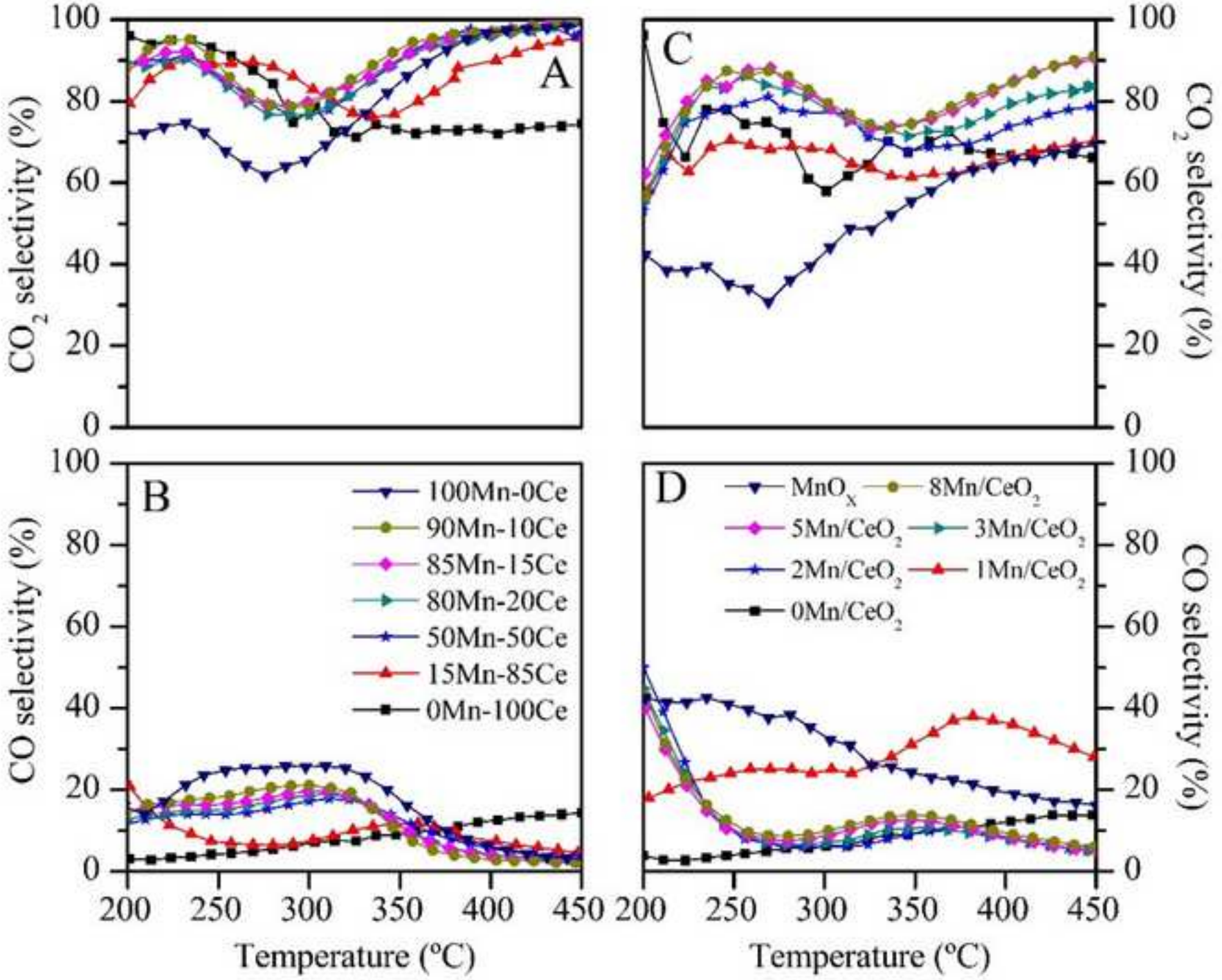

Figure 10

Click here to download high resolution image

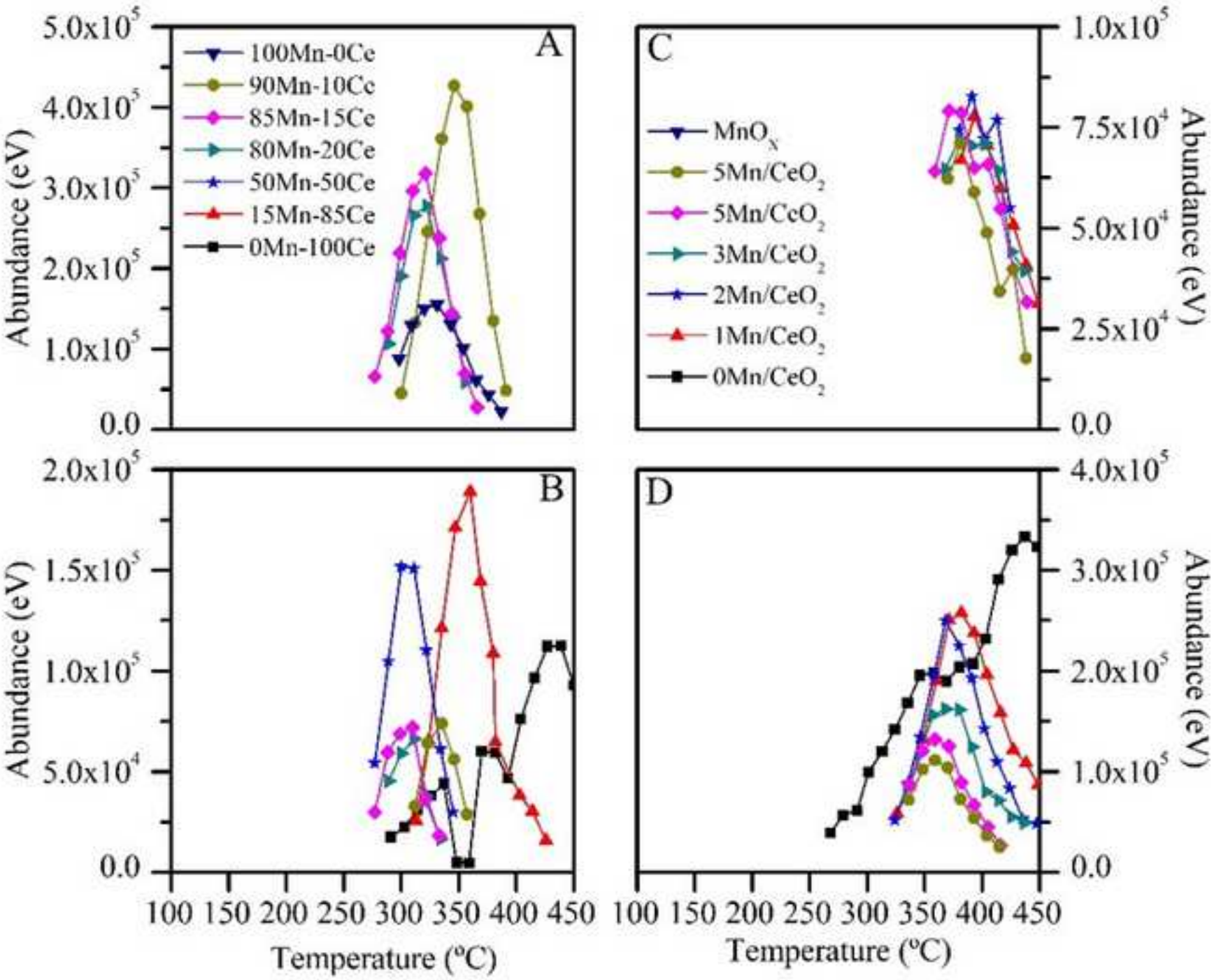

Figure 11

Click here to download high resolution image

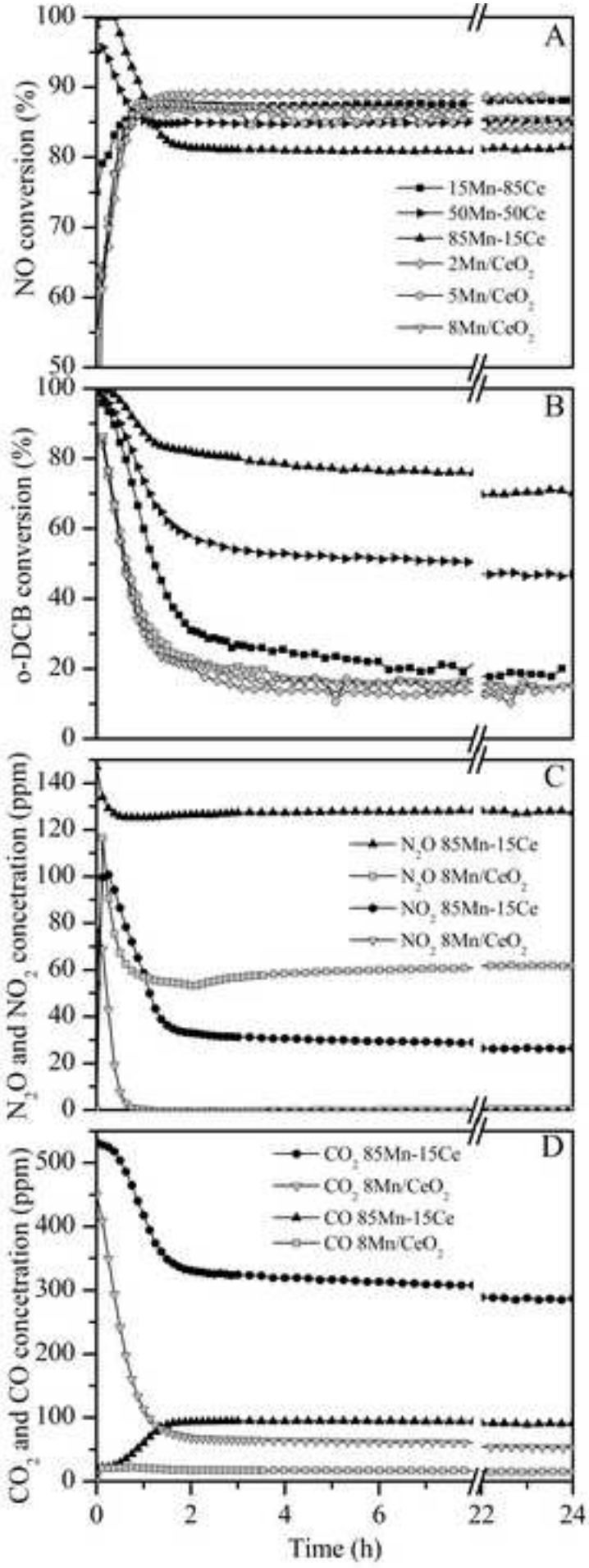

***Credit Author Statement**

J.A. Martín-Martín: Investigation, Methodology, Writing-Original Draft preparation. **J. Sánchez-Robles:** Investigation. **M.P. González-Marcos:** Conceptualization, Writing-Reviewing and Editing. **A. Aranzabal:** Conceptualization, Writing-Reviewing and Editing. **J.R. González-Velasco:** Supervision.

***Declaration of Interest Statement**

Declaration of interests

☒ The authors declare that they have no known competing financial interests or personal relationships that could have appeared to influence the work reported in this paper.

☐The authors declare the following financial interests/personal relationships which may be considered as potential competing interests: